Научном већу Института за физику

Београд, 25. октобар 2019.
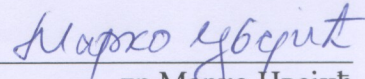
Предмет: Молба за покретање поступка за реизбор у звање научни сарадник

С обзиром да испуњавам критеријуме прописане од стране Министарства просвете,науке и технолошког развоја за реизбор у звање научни сарадник, молим Научно веће Института за физику у Београду да покрене поступак за мој реизбор у наведено звање.

У прилогу достављам:

1. Мишљење руководиоца пројекта са предлогом чланова комисије
2. Кратку биографију
3. Преглед научне активности
4. Елементе за квалитативну оцену научног доприноса
5. Елементе за квантитативну оцену научног доприноса
6. Списак објављених радова и њихове копије
7. Списак цитата

С поштовањем,

др Марко Цвејић

Научном већу Института за физику

Београд, 25. Октобар 2019.

Предмет: Мишљење руководиоца пројекта
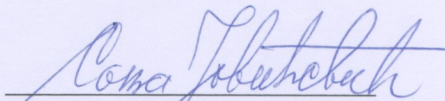## за реизбор др Марка Цвејића у звање <u>научни сарадник</u>

Др Марко Цвејић, запослен у Лабораторији за спектроскопију плазме и физику ласера, Института за физику ангажован је на пројектима: (1) из области основних истраживања ОИ171014 под насловом „Спектроскопска дијагностика нискотемпературне плазме и гасних пражњења: облици спектралних линија и интеракција са површинама"; (2) из области технолошког развоја ТР 37019 „Електродинамика атмосфере у урбаним срединама Србије". Оба пројекта финансира Министарство просвете, науке и технолошког развоја Републике Србије. На поменутим пројектима ради на теми спектроскопије ласерски индуковане плазме.

У протеклих 5 година био је на постдокторским студијама на институту Ваицмана у Израелу, у Плазма лабораторији код проф. Ицхака Марона, где је радио на експерименту З-пинча са уграђеним аксијалним магнетним пољем и бавио се проблематиком компресије магнетизоване плазме и магнетног поља.

С обзиром да испуњава све предвиђене услове, у складу са Правилником за изборе у научна звања Министарства, сагласна сам са покретањем поступка за реизбор др Марка Цвејића у звање научни сарадник.

За састав Комисије <u>за</u> реизбор др Марка Цвејића у звање научни сарадник предлажем:

1. др Соња Јовићевић, научни саветник, Институт за физику,

2. др Миливоје Ивковић, виши научни сарадник, Институт за физику,

3. др Јован Цветић, редовни професор, Електротехнички факултет факултет.

<div align="right">

Руководилац пројекта

др Соња Јовићевић

</div>

Биографија

Др. Марко Цвејић рођен је у Пожаревцу 09.08.1982. године. Пожаревачку гимназију завршио је 2001. године. У августу 2007. године, дипломирао је на Електротехничком факултету Универзитета у Београду, на смеру за Физичку електронику – одсек за Оптоелектронику и ласерску технику. Докторске студије на Електротехничком факултету у Београду, модул Наноелектроника и фотоника, уписао је 2008. године. Докторску дисертацију под називом „*Просторна и временски разложена спектроскопска дијагностика ласерски индуковане плазме на чврстој мети у ваздуху на атмосферском притиску*" одбранио је 26.09.2014. године.

Током основних студија учествовао је на пројекту израде Теслиног трансформатора и изложби о Николи Тесли поводом 150 година рођења у Галерији САНУ (2006). Од децембра 2007. до августа 2008. одслужио је цивилни војни рок. Од новембра 2008. до јуна 2009. године био је ангажован на Физичком факултету Универзитета у Београду на истраживању експеримента тињавог пражњења са микро шупљином, у лабораторији академика Николе Коњевића. Од 01.06.2009. године запослен је у Институту за физику у Лабораторији за спектроскопију плазме и физику ласера где је ангажован на експериментима тињавог пражњења на атмосферском притиску и експерименту спектроскопије ласерски индуковане плазме. Од јула 2009. до децембра 2010. године био је ангажован на пројекту „Нискотемпературне плазме и гасна пражњења: Радијативна својства и интеракција са површинама", које је финансирало Министарство за науку и технолошки развој Републике Србије. Од 2011. ангажован је на пројектима: (1) из области основних истраживања под насловом „*Спектроскопска дијагностика нискотемпературне плазме и гасних пражњења: облици спектралних линија и интеракција са површинама*"; (2) из области технолошког развоја „*Електродинамика атмосфере у урбаним срединама Србије*". Оба пројекта финансира Министарство просвете, науке и технолошког развоја Републике Србије. Од 19.10.2014. године налази се на усавршавању на пост-докторским студијама на престижном Weizmann Institute of Sciencey у Израелу, у плазма лаборатоји код проф. Ицхака Марона, где ради на истраживњу концепта З-пинч плазме у аксијалном магнетном пољу. Овај концепт је један од најперспективнијих путева ка остварењу нуклеарне фузије и веома интензивно се проучава у Сандиа националним лаборатојама (Sandia National Laboratories), Албукерки, САД, где се и налази највећи З-пинч плазма ексепримент на свету.

Др. Цвејић је своје знање проширио учествовањем на неколико билатерлних пројеката и посетама иностраним лабораторијама. У мају 2010. и октобару 2011, био је у научној посети лабораторији ЛП3 (Laboratoire Lasers, Plasmas et Procédés Photoniques, LP3 UMR 6182 CNRS - Université Aix-Marseille II Campus de Luminy, Marseille), учествовавши на пројекту „Measurements of Stark broadening parameters in laser-produced plasmas" финансираном од стране LaserLab-Europe (http://www.laserlab-europe.net/). У периоду јун-јул 2014. године посетио је Одсек за фотонику, Института за физику при Јагелонском универзитету у Кракову у Пољској, где је истраживао особине ласерски индуковане плазме помоћу технике Томсоновог расејања.

Др. Цвејић је у браку са др. Аном Лопатином од марта 2017. године. Супруга је научни радник у области микробиологије и генетике, ангажована на пост-докторским студијама на Weizmann Institute of Science. У августу 2018. године родио им се син Милан.

Преглед научне активности др Марка Цвејића

Научна активност др. Цвејића је усмерена на проучавање физике плазме и гасних пражњења методама спектроскопије плазме и Томсоновог расејања. У досадашњем раду, проучавао је:

- MHGD (Micro Hollow Gas Discharge) Тињаво пражњење у мирко шупљини,
- APGD (Atmospheric Preassure Glow Discharge) Тињаво пражњење на атмосферском притиску,
- LIBS (Laser Induced Breakdown Spectroscopy) Спектроскопија ласерски индуковане плазме које је била тема његове докторске дисертације,
- Експеримент З-пинч плазме у аксијалном магнетном пољу (Z-pinch plasma experiment with pre-embedded axial magnetic field).

У раду **[A1]** испитивана је дистрибиција магнетног поља у имплозији плазме која се налази у магнетном пољу, у оквиру експеримента З-пинча. Временски и просторно разложена спектроскопска мерења, која користе поларизациона својства Земановог ефекта, примењена су по први пут у овом експерименту. Мерења су показала да је азимутално магнетно поље у плазми која имплодира, чак и у присуству веома слабог аксијалног магнетног поља, значајно мањег интензитета од очекиваног, које се добија из односа јачине струје и полупречника плазме која имплодира користећи Амперов закон. Већи део струје тече кроз споро имплодирајућу плзаму, мале густине, која окружује главну плазму која имплодира. Неочекивани резултати из претходинх експериемнта из литературе, урађених на снажним инсталацијама, као на пример З-машина у Сандиа националним лабораторијама у САД, укључујући необјашњење спиралне плазма структуре у експерименту инерцијалне нуклеарне фузије, могу бити објашњени открићима у овом раду [A1]. Развој конфигурације force-free current је предложен као објашњење овог феномена.

У раду [Б1] је проучавана изотермичка равнотежа у ласерски индукованој плазми на алуминијумској мети у атмосфери аргона на притиску од 200 mbar, коришћењем методе која комбинује стандардно ласерско Томсоново расејање и анализу спектралне линије водоника Hα, над којом је Штарково ширење доминантно. Плазма је креирана коришћењем Nd:YAG ласерског импулса дужине трајања 4,5 ns, енергије 4 mJ, на таласној дужини од 1064 nm. Густина елекрона и електронска температура одређени су из дела спектра Томсоновог расејања који доминантно зависи од утицаја динамике електрона. Температура неутрала и јона (тежих честица у плазми) је добијена анализом спектралног облика Hα линије коришћењем теоријских профила добијених компјутерском симулацијом која укључује ефекат динамике јона на спектрални профил. У раду [Б1] је пронађено да постоји јака неравнотежа између температуре електрона и температуре тежих честица у плазми, током целе

еволуције ласерски индуковане плазме, што показује њене не-изотермалне особине. У исто време, према McWhirter-овом критеријуму, густина електрона је довољно висока за успостављање локалне термодинамиче равнотеже.

У раду [Б2] презентована је студија просторне и временске еволуције ласерски индуковане плазме на алуминијумској мети која се налази у води. Ласерска аблација узрокована је коришћењем ласерског импулса трајања 20 ns, на таласној дужини од 1064 nm. Карактеристике плазме измерене су коришћењем брзе фотографије, Шлирен техником и методом фотографије сенке, као и оптичком емисионом спектроскопијом. Резултати експериемента показују постојање две различите фазе у плазми, прва фаза која има трајање од око 500 ns након ласерског импулса, за којом настаје раст нове, секундарне плазме која настаје из центра ласерског кратера. Секундарна плазма развија се релативно споро унутар растућег мехура паре, а њена оптичка емисија траје неколико десетина микросекунди. У току каснијих фаза развоја мехура детектоване су вруће светлеће честице, заробљене мехуром. Први колапс мехура настаје након 475 микросекунди од ласерског импулса. Разлике у особинама плазме током ове две фазе еволуције су дискутоване, са акцентом на детекцију оптичког сигнала, јер је детекција од примарне важности за ЛИБС технику. У раду је демонстирано да се квалитет ЛИБС сигнала након једног ласерског импулса под водом, може значајно побољшати детектовањем само оптичке емисије секундарне фазе плазме, коришћењем релативно дугог временског сигнала за аквизицију оптичке емисије (гејт сигнал, трајања од 10-100 микросекунди). Резултати овог рада су веома битни за ЛИБС мерења у течним срединама, јер доказују да се добар аналитички сигнал може добити коришћењем наносекундног ласерском импулса добијеног из комерцијално доступног ласера и коришћењем приступачних детектора за које није потребно брзо гејтовање.

ЕЛЕМЕНТИ ЗА КВАЛИТАТИВНУ АНАЛИЗУ РАДА КАНДИДАТА

1. Показатељи успеха у научном раду

Др Марко Цвејић је од 24.10.2014. на стручном усавршавању на пост-докторским студијама на престижном Вајцман институту у Израелу, који је се налази међу 25 најбољих научних институција на свету (https://wis-wander.weizmann.ac.il/weizmann-institute-science-ranked-top-25) према категоризацији U-Multirank (https://www.umultirank.org/). Марко ради у Плазма лабораторији, Вајцман института, коју води проф. Ицхак Марон.

Од октобра 2017. награђен је статусом "senior postdoctoral fellow" за своје заслуге током редовног пост-докторског периода.

У децембру 2018 имао је предавање по позиву на APS-DPP (American Physical Society – Department for Plasma Physics) скупу.

Од октобра 2019. награђен је статусом гостујућег научника.

2. Ангажованост у развоју услова за научни рад, образовању и формирању научних кадрова

Плазма лабораторија Вајцманн института у Израелу тесно сарађује са водећим универзитетима и националним лабораторијама у САД, као нпр. Cornell University, University of California at San Diego, Princeton Plasma Physics Laboratory, Lawrence Livermore National Laboratory, Los Alamos National Laboratory, Sandia National Laboratories, National Ignition Facility. Током боравка на постдокторским студијама имао је прилике да блиско сарађује са исраживачима из горе поменутих лабораторија.

Др Марко Цвејић био члан комисије за одбрану докторске тезе др Маријане Гавриловић-Божић.

3. Квалитет научних резултата

Кандидат је у свом научном раду, од избора у претходно звање, објавио 3 рада у међународним часописима са ИСИ листе у категорији М20.

У категорији М21а кандидат је објавио 1 рад у Physical Review Letters (PRL) часопису (ИФ:9.227);

У категорији М21 кандидат је објавио 2 рада:

1 рад у Applied Physics Letters (ИФ:3.521)

1 рад у Physical Chemistry Chemical Physics (3.567).

Укуупан импакт фактор радова кандидата у горњим часописима је **16,315**. Према **Scopus**-u, научни радови др Марка Цвејића остварени у претходном периоду (2015-2019) су цитирани укупно 23 пута у међународним часописима од тога 21 пута без самоцитата.

This is an overview of citations for the documents you've selected.

Document *h*-index : 6   View *h*-graph ⑦

12 cited documents   ✛ Add to list

Date range: 2015 ▼ to 2019 ▼   ■ Exclude self citations of all authors   ☐ Exclude citations from books   Update
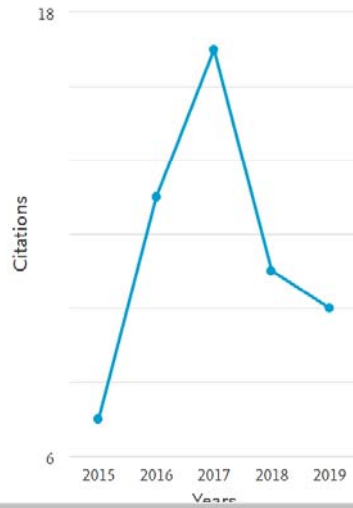
Documents	Citations	<2015	2015	2016	2017	2018	2019	Subtotal	>2019	Total
Total		33	7	13	17	11	10	58	0	91
☐ 1 Effects of a Preembedded Axial Magnetic Field on the Current...	2019							0		0
☐ 2 Current outflow to low-density plasma region of z-pinch with...	2018							0		0
☐ 3 Secondary plasma formation after single pulse laser ablation...	2016				8	3	5	16		16
☐ 4 Investigation of thermodynamic equilibrium in laser-induced ...	2015			2	1	2	2	7		7
☐ 5 The Beenakker's cavity for uniform column of nonequilibrium ...	2014							0		0
☐ 6 Neutral lithium spectral line 460.28 nm with forbidden compo...	2014		1	2		2		5		5
☐ 7 Diagnostics of laser-induced plasma by optical emission spec...	2014					1		1		1
☐ 8 Stark broadening measurement of Al II lines in a laser-induc...	2014	4	3	4	4	2	1	14		18
☐ 9 Stark broadening of Mg i and Mg II spectral lines and Debye ...	2013	10	2	1	2	1	2	8		18
☐ 10 Spectroscopic diagnostics of microhollow gas discharge in hy...	2012	3		1	1			2		5
☐ 11 A contribution to spectroscopic diagnostics and cathode shea...	2011	7	1	2				3		10
☐ 12 Simultaneous plasma and electric field diagnostics of microd...	2010	9		1	1			2		11

Display: 20 ▼ results per page   1   ⌃ Top of page

ЕЛЕМЕНТИ ЗА КВАНТИТАТИВНУ АНАЛИЗУ РАДА КАНДИДАТА

Др Марка Цвејића за реизбор у звање научни сарадник

Остварени резултати у периоду 2015-2019, периоду пре реизбора, након избора у претходно звање

Категорија	М бодова по раду	Број радова	Укупно М бодова
М21а	10	1	10
М21	8	2	16
М32	1,5	1	1,5
М33	1	1	1
М34	0,5	13	6,5

Поређење са минималним квантитативним условима за избор у звање научни сарадник

Минимални број М бодова	Неопходно	Остварено
Укупно	16	34
М10+М20+М31+М32+М33+М41+М42	10	34
М11+М12+М21+М22+М23	6	26

Списак радова др Марка Цвејића у периоду 2015-2019

А. РАД У МЕЂУНАРОДНОМ ЧАСОПИСУ ИЗВАНДРЕДНЕ ВРЕДНОСТИ (М21А)

[А1] D. Mikitchuk, **M. Cvejić**, R. Doron, E. Kroupp, C. Stollberg, Y. Maron, A.L. Velikovich, N.D. Ouart, J.L. Giuliani, T.A. Mehlhorn, E.P. Yu, and A. Fruchtman; *Effects of a preembedded axial magnetic field on the current distribution in a Z-pinch implosion* (2019) Phys. Rev. Lett. 122, 045001
DOI: 10.1103/PhysRevLett.122.045001 **(дељено ауторство са D. Mikitchuk као првим аутором)**

Б. РАДОВИ У ВРХУНСКИМ МЕЂУНАРОДНИМ ЧАСОПИСИМА (М21)

[Б1] **M. Cvejić,** Krzysztof Dzierzega, T. Pięta; *Investigation of the thermodynamic equilibrium in laser-induced aluminum plasma using the Hα line profiles and Thomson scattering spectra* (2015) Applied Physics Letters, 107, 024102-1
DOI: 10.1063/1.4926990

[Б2] M.R. Gavrilović, **M. Cvejić** , V. Lazic and S. Jovićević; *Secondary plasma formation after single pulse laser ablation underwater and its advantages for laser induced breakdown spectroscopy (LIBS)* (2016) Physical Chemistry Chemical Physics, 18, 14629- -14637
DOI: 10.1039/C6CP01515H

В. ПРЕДАВАЊЕ ПО ПОЗИВУ СА МЕЂУНАРДОНОГ СКУПА ШТАМПАНО У ИЗВОДУ(М32)

[В1] **M. Cvejić**, *Current re-distribution in an experiment of magnetic flux compression by an imploding plasma*, **invited talk** at the APS-DPP-2018 (American Physical Societe - Division of Plasma Physics),
http://meetings.aps.org/Meeting/DPP18/Session/CI2.3

Г. РАДОВИ САОПШТЕНИ НА СКУПУ МЕЂУНАРОДНОГ ЗНАЧАЈА ШТАМПАНИ У ЦЕЛИНИ (М33)

[Г1] **M. Cvejić**, D. Mikitchuk, R. Doron, E. Kroupp, C. Stollberg, Y. Maron, *Current distribution in an experiment of z-pinch with pre-embedded axial magnetic field*, the 29th Summer School and International Symposium on the Physics of Ionized Gases (SPIG 2018), August 28, September 1, 2018, Belgrade, Serbia, p.146-149

Д. РАДОВИ САОПШТЕНИ НА СКУПУ МЕЂУНАРОДНОГ ЗНАЧАЈА ШТАМПАНИ У ИЗВОДУ (М34)

[Д1] **M. Cvejić**, E. Stambulchik, M.R.Gavrilović, S. Jovićević, N. Konjević, *Neutral Lithium Spectral Line 460.28 nm with Forbidden Component for Low Temperature Plasma Diagnostics of Laser-Induced Plasma*, IPSTA-2015, Ariel University

[Д2] **M. Cvejić**, T. Pięta, M.R. Gavrilović, S. Jovicević and K. Dzierżęga, *Investigations of Hα line profile in laser - induced plasma using Thomson scattering and optical emission methods*, 3rd Spectral Line Shapes in Plasmas Workshops (SLSP), Marseille 2015

[Д3] M.R. Gavrilović, **M. Cvejić**, V. Lazić, S. Jovićević, *Diagnostics of underwater laser-induced breakdown on alumina target*, 8th Euro-mediterranean Symposium on Laser-Induced Breakdown Spectroscopy (EMSLIBS), Linz 2015.

[Д4] D. Mikitchuk, R. Doron, **M. Cvejić**, E. Kroupp, Y. Maron, *Method for spatially resolved magnetic field measurements in plasmas using laser produced dopant*, 8th Euro-mediterranean Symposium on Laser-Induced Breakdown Spectroscopy (EMSLIBS), Linz 2015

[Д5] **M. Cvejić**, T. Pięta, K. Dzierżęga, *Diagnostics of laser-induced aluminum plasma using Hα line profiles and Thomson scattering spectra: Investigation of isothermal equilibrium*, 8th Euro-mediterranean Symposium on Laser-Induced Breakdown Spectroscopy (EMSLIBS), Linz 2015.

[Д6] **Marko Cvejić**, Dmitry Mikitchuk, Eyal Kroupp, Ramy Doron and Yitzhak Maron, *Determination of the azimuthal magnetic field evolution in imploding magnetized plasma*, 19th Israeli Conference on Plasma Science, Jerusalem, 2017

[Д7] A. L. Velikovich, N. D. Ouart, J. L. Giuliani, R. B. Baksht, A. G. Rousskikh, V. I. Oreshkin, D. Mikitchuk, **M. Cvejic**, R. Doron, E. Kroupp, and Y. Maron, "Force-Free Current Flow in Z Pinches Imploded in an Axial Magnetic Field*," 2017 IEEE International Conference on Plasma Science (ICOPS), Atlantic City, NJ, 2017, pp. 1-1.
doi: 10.1109/PLASMA.2017.8496380

[Д8] Dimitry Mikitchuk, **Marko Cvejic**, Eyal Kroupp, Ramy Doron, Yitzhak Maron, Alexander L. Velikovich, John L. Giuliani, *Magnetic-field evolution in Z-pinch implosion with preembedded axial magnetic field*, Pulsed Power Conference (PPC), Brighton, 2017

[Д9] **Marko Cvejić,** Dimitry Mikitchuk, Ramy Doron, Eyal Kroup, and Yitzhak Maron, *Spectroscopic measurements of z-pinch implosion with pre-embedded axial magnetic field*, 20th Israeli Conference on Plasma Science, Tel Aviv, 2018

[Д10] D. Mikitchuk, **M. Cvejić**, R. Doron, E. Kroupp, C. Stollberg, Y. Maron, A.L. Velikovich, N.D. Ouart, J.L. Giuliani, T.A. Mehlhorn, E.P. Yu, and A. Fruchtman, *Effects of axial magnetic field on the current distribution in Z-pinch implosion with pre-embedded axial*

magnetic field, The 45th IEEE International Conference on Plasma Science (ICOPS 2018), Denver, 2018

[Д11] M. Cvejić, D. Mikitchuk, R. Doron, E. Kroupp, C. Stollberg, Y. Maron, A.L. Velikovich, N.D. Ouart, J.L. Giuliani, T.A. Mehlhorn, E.P. Yu, and A. Fruchtman, *Current outflow to low-density plasma region of z-pinch with pre-embedded axial magnetic field*, The 45th European Physical Society Conference on Plasma Physics (EPS2018), Prague, 2018

[Д12] Christine Stollberg , Eyal Kroupp, Dmitry Mikitchuk , **Marko Cvejic**, Ramy Doron, Evgeny Stambulchik , Y. Maron, Amnon Fruchtman , Uri Shumlak, John Giuliani, *Direct observation of the current evolution in a small-scale self-compressing plasma column*, IEEE PULSED POWER AND PLASMA SCIENCE CONFERENCE 2019 23-28 June 2019 Orlando, Florida

[Д13] Marko Cvejić, Dimitry Mikitchuk, Eyal Kroupp, Ramy Doron, Yitzhak Maron, Uri Shumlak, *Ion velocities measurements in Z-pinch with pre-embedded axial magnetic field,* IVS-IPSTA 2019 - 37th Annual Conference and Workshop/Haifa Sept 3rd 2019/

Investigation of thermodynamic equilibrium in laser-induced aluminum plasma using the H α line profiles and Thomson scattering spectra

M. Cvejić, K. Dzierżęga, and T. Pięta

Articles you may be interested in

Stark broadening for diagnostics of the electron density in non-equilibrium plasma utilizing isotope hydrogen alpha lines
J. Appl. Phys. 115, 163106 (2014); 10.1063/1.4873960

Electron temperature and density determination in a nonequilibrium laser induced plasma by means of self-reversed-line spectroscopy
Appl. Phys. Lett. 93, 041501 (2008); 10.1063/1.2963472

Spectroscopic characterization of laser-induced tin plasma
J. Appl. Phys. 98, 013306 (2005); 10.1063/1.1977200

Characteristics of an atmospheric microwave-induced plasma generated in ambient air by an argon discharge excited in an open-ended dielectric discharge tube
Phys. Plasmas 9, 4045 (2002); 10.1063/1.1495872

Plasma broadened 419.07 nm and 419.10 nm neutral argon lines
AIP Conf. Proc. 467, 191 (1999); 10.1063/1.58308

Investigation of thermodynamic equilibrium in laser-induced aluminum plasma using the Hα line profiles and Thomson scattering spectra

M. Cvejić,[1,2,a)] K. Dzierżęga,[3,a)] and T. Pięta[3]

[1]*Institute of Physics, University of Belgrade, P.O. Box 68, 11080 Belgrade, Serbia*
[2]*Faculty of Physics, Weizmann Institute of Science, Rehovot 7610001, Israel*
[3]*M. Smoluchowski Institute of Physics, Jagellonian University, ul. Łojasiewicza 11, 30-348 Kraków, Poland*

We have studied isothermal equilibrium in the laser-induced plasma from aluminum pellets in argon at pressure of 200 mbar by using a method which combines the standard laser Thomson scattering and analysis of the Hα, Stark-broadened, line profiles. Plasma was created using 4.5 ns, 4 mJ pulses from a Nd:YAG laser at 1064 nm. While electron density and temperature were determined from the electron feature of Thomson scattering spectra, the heavy particle temperature was obtained from the Hα full profile applying computer simulation including ion-dynamical effects. We have found strong imbalance between these two temperatures during entire plasma evolution which indicates its non-isothermal character. At the same time, according to the McWhirter criterion, the electron density was high enough to establish plasma in local thermodynamic equilibrium. © 2015 AIP Publishing LLC. [http://dx.doi.org/10.1063/1.4926990]

A detailed description of laser-induced plasma (LIP), important for modeling and analytical purposes, requires a thorough knowledge of atom, ion, and free electron number densities and their temperatures. These parameters are usually determined in an indirect way from optical emission measurements, assuming plasma in local thermodynamic equilibrium (LTE). Such assumption always needs careful verification, not easy in case of LIP of transient character and with large spatial gradients. The concept of LTE has various nontrivial aspects which were discussed by van der Mullen[1,2] and recently recalled by Christoforetti *et al.*[3] for the case of LIP. Among others, two balances—Saha-Boltzmann and isothermal—must be locally in equilibrium. This condition is usually verified comparing excitation and de-excitation rates of inelastic electron collisions with respective radiative ones, and it is expressed by the minimal electron number density n_e^W (Ref. 3)

$$n_e(\text{m}^{-3}) > n_e^W = 2.55 \times 10^{17} \frac{T_e^{1/2}\Delta E^3}{\langle \bar{g} \rangle}, \qquad (1)$$

often called the McWhirter criterion where $\langle \bar{g} \rangle$ is the Gaunt factor averaged over the electron energy distribution function. T_e and ΔE, expressed respectively in K and eV, stand for electron temperature and the largest energy gap between adjacent levels, usually between the ground and the first excited ones coupled by the electric dipole transition. Besides the Saha-Boltzmann equilibrium, LTE also assumes equal temperatures of electrons and heavy particles (T_i).

The purpose of the present work is to study the local thermal equilibrium in laser-induced plasma by combination of the direct measurements of the electron number density, T_e and T_i, using the laser Thomson scattering (TS) method with the analysis of the hydrogen Hα Stark-broadened profiles. The only experiment in which both T_e and T_i in LIP

were studied was carried out by Dzierżęga *et al.*[4] Applying Thomson and Rayleigh scattering, they showed non-isothermal character of helium LIP at atmospheric pressure. The local Saha-Boltzmann equilibrium (LSBE) in Al LIP in ambient air was recently studied by Mendys *et al.*[5] also using the TS technique. With thorough analysis of temporal and spatial distribution of n_e and T_e, they showed Al atoms and ions to fulfill the LSBE conditions during most of plasma evolution while the McWhirter criterion was never satisfied for N species.

In TS method, n_e and T_e are directly derived from the electron feature of the TS spectrum without any assumptions about the plasma chemical composition or its equilibrium state unlike T_e determined from emission spectra with the use of the Boltzmann graph method. The spectrum of photons from the incident laser beam of a wavelength λ_L, scattered on plasma electrons, is described by the spectral density function $S(\Delta\lambda)$ with $\Delta\lambda = \lambda - \lambda_L$. The character of TS and its spectrum are governed by the scattering parameter $\alpha \equiv (\lambda_L/\sin(\theta/2))(n_e/T_e)^{1/2}$ where θ stands for observation angle with respect to the direction of the incident laser beam. In case of the so called collective or partially collective ($\alpha \geq 1$) scattering, $S(\Delta\lambda)$ takes the form of two satellites with their widths depending on T_e and their separation related to both T_e and n_e. These characteristics of the TS spectra thus enable one to unambiguously determine the electron density and temperature in the plasma, and they are presented in Fig. 1 for plasma parameters typical for LIP at early stages of its evolution.[7]

The hydrogen Hα, Stark-broadened, line profiles (mostly its full widths at half maximum—FWHM) are a well-established diagnostics tool in plasma physics for n_e determination.[8] However, it is well-known that so called ion-dynamical effects can significantly modify their full profiles.[10] These effects explain large discrepancies appearing between the measured profiles and the calculated with the use of models considering ions as static particles.[11,12] The ion-dynamical

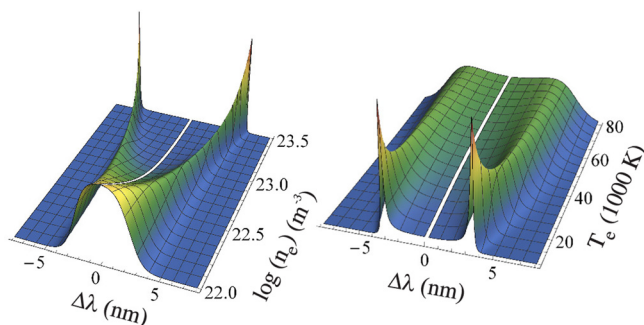a)Electronic mail: marko.cvejic@ipb.ac.rs and krzysztof.dzierzega@uj.edu.pl

FIG. 1. The electron feature of the spectral density function of the Thomson scattering modelled for the observation perpendicular to the incident laser beam of $\lambda_L = 532$ nm, for constant $T_e = 20000$ K (left) and constant $n_e = 1.0 \times 10^{23}$ m^{-3} (right). The scattering parameter α varies from 0.61 to 3.45 and from 2.74 to 0.97 in the left and right figures, respectively. Calculations performed according to Evans and Katzenstein.[6]

effects result from the relative motion of the emitter (hydrogen)–perturber (ion) pair with $\langle v_{rel} \rangle^2 = 2kT_H/m_H + 2kT_i/m_i$. Under assumption of a two-temperature plasma ($T_e \neq T_H = T_i$), these effects are accounted for with the concept of the reduced mass $\mu^{-1} = m_H^{-1} + m_i^{-1}$.[10]

Figure 2 shows hydrogen H$_\alpha$ line widths depending on the imbalance between ion (heavy particle) and electron temperatures for given n_e and T_e. Calculations were performed using the data presented by Gigosos et al.[9] based on computer simulations including ion-dynamical effects and non-equilibrium plasma. Although the full width at half area (FWHA) is very weekly affected by ion-dynamics, the other two widths, $\Delta\lambda_{1/2}$ (at half of the maximum) and $\Delta\lambda_{1/8}$ (at one eigths of the maximum), reveal quite significant sensitivity to the particles kinetics. Moreover, the line wings (see $\Delta\lambda_{1/8}/\Delta\lambda_{1/2}$) become broader as the imbalance in temperatures increases. The latter feature of the H$_\alpha$ line profile was exploited in the work of Gonzalez and Gigosos[13] and now in our investigations of aluminium LIP assuming the electron density and temperature as determined from TS experiment.

The scheme of the experimental setup is shown in Fig. 3, and its details have been described in our recent paper.[7] Briefly, a vacuum chamber was evacuated below 0.1 mbar and then purged with argon at 200 mbar at a constant flow rate of 30 l/h. Plasma was generated by a Q-switched
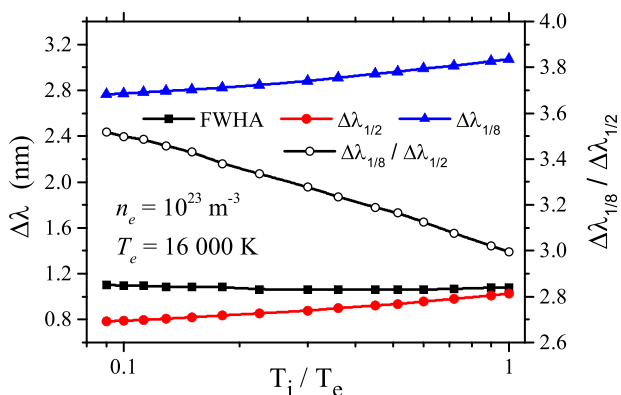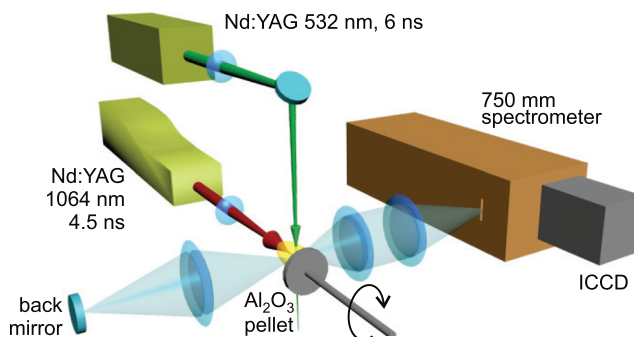

FIG. 3. Scheme of the experimental setup.

Nd:YAG laser (1064 nm, 4mJ), operating at a repetition rate of 10 Hz, with a pulse duration of 4.5 ns. The laser beam was focused 1 mm behind front surface of continuously rotated target sample, yielding ablating pulses with fluence of 45 J/cm^2 (10^{10} W/cm^2). The target was alumina pellets (Al$_2$O$_3$) containing some adsorbed H$_2$O vapors. All experimental parameters were matched to have shot to shot highly reproducible plasma plume. For laser TS, a separate, single mode ($\Delta\lambda < 0.28$ pm), Nd:YAG laser with 6.0 ns pulse duration at 532 nm was used. This laser beam was directed orthogonally to the first, plasma generating one, and was polarized perpendicularly to the observation direction. It was then focused in the plasma volume to the spot of about 200 μm in radius and laser pulses of 19 J/cm^2 fluence, lower than the ablation threshold, were applied. The delay between the pulses was controlled by a digital delay pulse generator with accuracy better than 0.5 ns.

The emission from LIP and the laser-scattering light were observed in a direction perpendicular to the plane of laser beams by imaging the investigated plasma plume onto the entrance slit of a Czerny-Turner spectrograph (750 mm focal length, 1.005 nm/mm reciprocal dispersion) with 1.2 magnification. Plasma imaging was performed using the zeroth order of the spectrograph with the entrance slit fully opened. Imaging allowed verification of the plasma stability and selection of its regions for further investigations. The spectra of the scattered light and the LIP emission were recorded over a wavelength range of 13.3 nm with slit widths of 50 μm and 30 μm, respectively. The instrumental profile for the emission part of the experiment was measured using a low pressure Hg spectral lamp and is well described by the Voigt function with equal Gaussian and Lorentzian contributions of 0.03 nm (FWHM) each. Self absorption of the studied H$_\alpha$ line was verified with the back-reflecting mirror method as it is described, e.g., in Cvejić et al.[14] In order to probe the specific layers of the plasma plume along its axis, the focusing lens and the pellet holder were mounted on two separate translation stages which were moved by the same distance to maintain laser fluence on surface of the sample.

The optical signals were collected using a gated two-dimensional intensified charge-coupled device (ICCD) camera with gate width synchronized to the probe and plasma-generating pulses in case of TS and emission measurements, respectively. In order to improve the signal-to-noise ratio of TS spectra, the ICCD gate width was as short as 6 ns. On the other hand, emission signals were recorded

FIG. 2. H$_\alpha$ broadening parameters vs. the ion temperature for $n_e = 10^{23}$ m^{-3} and $T_e = 16000$ K. Results obtained for a reduced mass of the emitter-perturber pair $\mu = 0.9$ in hydrogen mass units using the data presented by Gigosos et al.[9]
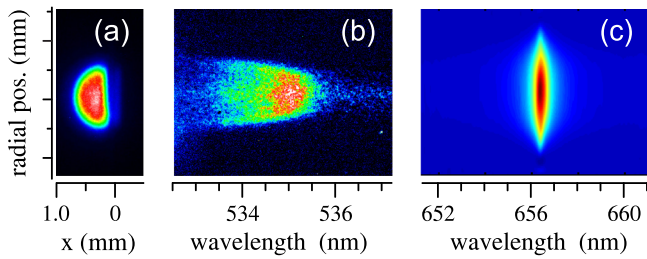
FIG. 4. Experimental results for LIP 1200 ns after ablating laser pulse. (a) Plasma image with the origin at the target surface, (b) TS spectrum after subtraction of plasma emission background while illuminatng plasma layer 0.6 mm away from surface of the sample, and (c) H_α spectrum (after Abel inversion) from the same LIP layer as in (b).
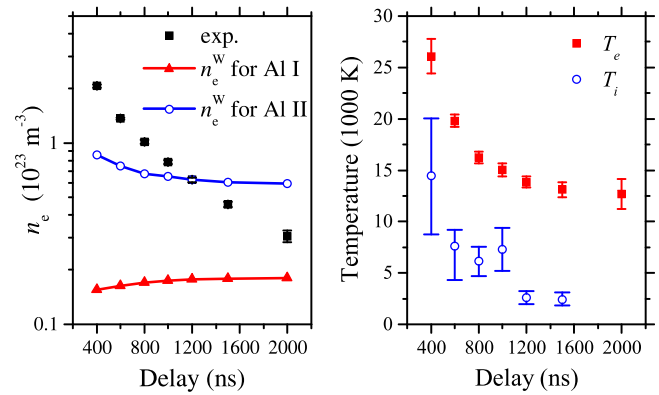

FIG. 6. Temporal evolution of electron and heavy particle temperatures, electron density, and of minimal n_e^W required to satisfy the McWhirter criterion. Results obtained on the axis of the plasma plume. The error bars for n_e are smaller than the size of the symbol.

setting this gate width to 3% of the respective delay time, e.g., 36 ns for 1200 ns delay, to have plasma of constant parameters. Laser scattered and emission spectra were averaged, respectively, over 2000 and 5000 laser shots and were investigated in the time interval from 400 ns to 2000 ns after plasma-generating laser pulse and from plasma layers 0.6 mm to 0.9 mm from the target surface. In case of TS measurements, a razor edge filter was placed in front of the spectrograph, to block radiation below 533.0 nm, in order to protect the ICCD from saturation by strong stray laser light scattered off the sample surface and its mount. The sensitivity of the whole experimental system was corrected for, pixel by pixel of the ICCD, using a halogen-deuterium lamp.

In Fig. 4(a), we present the LIP image recorded 1200 ns after the ablating pulse where the axial position $x = 0.0$ mm corresponds to the surface of the sample. Fig. 4(b) depicts the long-wavelength TS spectrum, after subtraction of the plasma background, collected while illuminating plasma layer 0.6 mm from the sample. This TS spectrum, with distinct electron feature, reveals partially collective character, and fitting the spectral density function $S(\Delta\lambda)$ directly yields electron density and electron temperature.[7] The example of the experimental TS spectrum, as obtained for the plasma axis, and the fitted $S(\Delta\lambda)$ is presented in Fig. 5(a). Radially resolved (across plasma plume) LIP emissivity, in the spectral range of the H_α line, observed at the same plasma conditions as for TS, is presented in Fig. 4(c). These spectra are determined from the original, laterally integrated emission spectra, applying inverse Abel transformation. Before Abel transformation was performed, the original data were corrected for dark current of the ICCD, the self-absorption (if

necessary), and, finally, they were smoothed using Savitzky-Golay filtering function.

The radially resolved H_α profiles were then fitted using computer simulation data as provided by Gigosos et al.[9] Under our experimental conditions, we assumed reduced mass of the emitter-perturber pair $\mu^{-1} = m_H^{-1} + m_{Al^+}^{-1}$, resulting in $\mu \cong 0.96$ in hydrogen mass units. The Stark profile was convoluted with the Voigt profile including the instrumental and the Doppler broadenings. The final fitting was performed at given n_e and T_e, as determined from the TS experiment, while varying T_i. The result for some sample data is shown in Fig. 5(b), where electron temperature significantly exceeds heavy particles' temperature. This indicates plasma out of isothermal equilibrium. Although reasonable agreement between the experimental and theoretical profiles can also be obtained assuming isothermal plasma conditions (see Fig. 5(c)), the resulting electron densities strongly deviate from values determined in independent TS experiments. In each case we studied, this discrepancy was larger than the combined uncertainty limits of TS and H_α measurements which further supports conclusion about non-isothermal plasma displayed through ion-dynamical effects. The temporally resolved (during plasma evolution) n_e, T_e, and T_i are presented in Fig. 6. The electron density decreases from 2.1×10^{23} m^{-3} at 400 ns to 3.1×10^{22} m^{-3} at 2 μs after the ablating pulse. At the same time, the measured electron temperature drops from about 26100 K to about 12700 K and largely exceeds the heavy particle (ion) temperature which
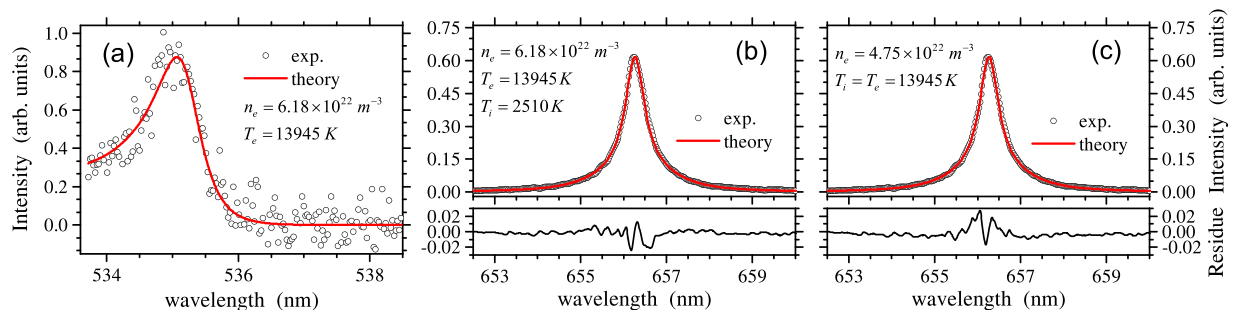

FIG. 5. Thomson scattering spectrum fitted with the spectral density function $S(\Delta\lambda)$ (a). H_α profile fitted assuming non-isothermal plasma conditions and using n_e and T_e from TS experiment, $r^2 = 0.99901$ (b) and assuming isothermal plasma with T_e as obtained from TS experiment, $r^2 = 0.9988$ (c). All results correspond to the axis of the plasma at 1200 ns after ablating laser pulse.

decreases from 14480 K to 2410 K. The large discrepancy between T_e and T_i exists for the entire plasma evolution studied in this work which indicates its non-isothermal character, despite the McWhirter criterion is satisfied (at least until 1.2 μs) for both aluminum atoms and ions (see Fig. 6).

In summary, we have shown that combination of standard spectroscopic methods—the laser Thomson scattering and analysis of H$_\alpha$ Stark-broadened line profiles—can provide reliable results about plasma, independent of its equilibrium state. Such joint method should be useful in studies of non-thermal plasmas and LIP in particular. We also conclude that in case of non-thermal plasmas, the electron number density cannot be derived from the FWHM of the H$_\alpha$ line profile, instead its FWHA is recommended.

[1]A. M. van der Mullen, "On the atomic state distribution function in inductively coupled plasmas—I. Thermodynamic equilibrium considered on the elementary level," Spectrochim. Acta Part B **44**, 1067–1080 (1989).

[2]A. M. van der Mullen, "On the atomic state distribution function in inductively coupled plasmas—II. The stage of local thermal equilibrium and its validity region," Spectrochim. Acta Part B **45**, 1–13 (1990).

[3]G. Cristoforetti, A. D. Giacomo, M. Dell'Aglio, S. Legnaioli, E. Tognoni, and N. O. V. Palleschi, "Local thermodynamic equilibrium in laser-induced breakdown spectroscopy: Beyond the McWhirter criterion," Spectrochim. Acta Part B **65**, 86–95 (2010).

[4]K. Dzierżęga, A. Mendys, B. Pokrzywka, W. Zawadzki, and S. Pellerin, "Simultaneous measurement of electron and heavy particle temperatures in He laser-induced plasma by Thomson and Rayleigh scattering," Appl. Phys. Lett. **102**, 134108 (2013).

[5]A. Mendys, M. Kanski, A. Farah-Sougueh, S. Pellerin, B. Pokrzywka, and K. Dzierżęga, "Investigation of the local thermodynamic equilibrium of laser-induced aluminum plasma by thomson scattering technique," Spectrochim. Acta Part B **96**, 61–68 (2014).

[6]O. E. Evans and J. Katzenstein, "Laser light scattering in laboratory plasmas," Rep. Prog. Phys. **32**, 207–271 (1969).

[7]K. Dzierżęga, A. Mendys, and B. Pokrzywka, "What can we learn about laser-induced plasmas from Thomson scattering experiments," Spectrochim. Acta Part B **98**, 76–86 (2014).

[8]H. R. Griem, *Principles of Plasma Spectroscopy*, 2nd ed. (Cambridge University Press, 1997).

[9]M. A. Gigosos, M. A. Gonzalez, and V. Cardenoso, "Computer simulated Balmer-alpha, -beta, and -gamma Stark line profiles for non-equilibrium plasma diagnostics," Spectrochim. Acta Part B **58**, 1489–1504 (2003).

[10]J. Seidel and R. Stamm, "Effects of radiation motion on plasma-broadened hydrogen Lyman-β," J. Quant. Spectrosc. Radiat. Transfer **27**, 499–503 (1982).

[11]W. L. Wiese, D. E. Kelleher, and D. R. Paquette, "Detailed study of the stark broadening of Balmer lines in a high-density plasma," Phys. Rev. A **6**, 1132–1153 (1972).

[12]M. A. Gigosos, "Stark broadening models for plasma diagnostics," J. Phys. D: Appl. Phys. **47**, 343001 (2014).

[13]M. A. Gonzalez and M. A. Gigosos, "Analysis of Stark line profiles for non-equilibrium plasma diagnostics," Plasma Sources Sci. Technol. **18**, 034001 (2009).

[14]M. Cvejić, M. R. Gavrilović, S. Jovicević, and N. Konjević, "Stark broadening of Mg I and Mg II spectral lines and Debye shielding effect in laser induced plasma," Spectrochim. Acta Part B **85**, 20–33 (2013).

PCCP

PAPER

CrossMark
click for updates

Secondary plasma formation after single pulse laser ablation underwater and its advantages for laser induced breakdown spectroscopy (LIBS)

M. R. Gavrilović,[ab] M. Cvejić,[a] V. Lazic[c] and S. Jovićević*[a]

In this work we present studies of spatial and temporal plasma evolution after single pulse ablation of an aluminium target in water. The laser ablation was performed using 20 ns long pulses emitted at 1064 nm. The plasma characterization was performed by fast photography, the Schlieren technique, shadowgraphy and optical emission spectroscopy. The experimental results indicate the existence of two distinct plasma stages: the first stage has a duration of approximately 500 ns from the laser pulse, and is followed by a new plasma growth starting from the crater center. The secondary plasma slowly evolves inside the growing vapor bubble, and its optical emission lasts over several tens of microseconds. Later, the hot glowing particles, trapped inside the vapor cavity, were detected during the whole cycle of the bubble, where the first collapse occurs after 475 μs from the laser pulse. Differences in the plasma properties during the two evolution phases are discussed, with an accent on the optical emission since its detection is of primary importance for LIBS. Here we demonstrate that the LIBS signal quality in single pulse excitation underwater can be greatly enhanced by detecting only the secondary plasma emission, and also by applying long acquisition gates (in the order of 10–100 μs). The presented results are of great importance for LIBS measurements inside a liquid environment, since they prove that a good analytical signal can be obtained by using nanosecond pulses from a single commercial laser source and by employing cost effective, not gated detectors.

1 Introduction

Laser induced breakdown spectroscopy (LIBS) is based on plasma generation by short and intense laser pulses focused on solid, liquid or gaseous samples. Presently, LIBS is the only available technique for direct elemental analysis of bulk liquids and submerged targets. Single pulse (SP) laser excitation underwater has proven to be very challenging for LIBS due to several factors related to the plasma formation and de-excitation. Compared to the plasma initiation and development in a gaseous environment, the energy losses are much more pronounced when working inside a water environment. Before reaching the target, a certain amount of laser energy will be absorbed along the optical path through the water.[1,2] The laser induced plasma emission also suffers from the absorption before reaching the detector, particularly in the UV region. For that reason, the optical paths through water should be minimized by employing short focal lengths both for the beam focusing and the plasma

light collection. Dissolved particles or those generated after the laser ablation scatter the light and can also act as preferential breakdown sites, which screen the target from the incoming laser beam.[3,4] The importance of choosing the right focusing conditions when dealing with laser ablation (LA) underwater was elaborated by Nguyen *et al.*,[5] postulating the existence of an optimal focal position for the stable and reproducible plasma. However, even when the optimal conditions for ablation are established, a great deal of laser energy is spent on the liquid vaporization which strongly reduces the energy available for the plasma excitation.[6] Furthermore, the initially formed plasma has a very high electron density and shields the target from the remnant portion of the laser pulse. A portion of the total laser energy absorbed by the plasma is dependent on the focusing conditions, the laser wavelength, the pulse duration and the irradiance.[7] With ns pulses at 1064 nm, more than 90% of the input laser energy could be absorbed by the plasma.[7,8] From one side, this fact is favourable for the plasma excitation but on the other, it decreases the effective irradiance on the submerged target and reduces the ablation rate.

Laser ablation and plasma inside liquids are highly affected by confinement with high density media,[9] followed by the

a Institute of Physics, University of Belgrade, 11081 Belgrade, P.O. Box 68, Serbia.
  E-mail: jovicevic@ipb.ac.rs
b Faculty of Electrical Engineering, University of Belgrade, 11120 Belgrade, Serbia
c ENEA (FSN-TECFIS-DIM), Via. E. Fermi 45, 00044 Frascati (RM), Italy

emission of intense shock waves and vapour bubble formation. The cavitation bubble, containing hot plasma and vapour, expands from the plasma site. Initially, the bubble has very high inner pressure and temperature, which decrease during the cavity expansion both due to volume enlargement and vapour condensation across the bubble–liquid interface. When the bubble reaches the maximum radius, its pressure is reduced to a saturated vapour pressure of the liquid. Since this inner pressure is much lower than the pressure of the surrounding liquid, the bubble starts to shrink until the rate of condensation cannot offset the volumetric reduction. The collapse of bubbles on a submerged target leads to a rapid increase of the inside gas temperature and pressure which induce an additional expulsion of the target material,[10] a subsequent release of the second shock wave and re-expansion of the bubble. Depending on the energy stored in the bubble, its oscillation may continue for several cycles of expansion and collapse.[11,12] Bubble formation and the plasma confinement inside liquids are responsible for large differences between plasma formation in gases and liquids. High acoustic pressure and long duration shockwave in liquids with respect to a gas environment lead to a manifold increase of the LA efficiency and also to lowering of the ablation threshold.[13] Although the ablation rates inside liquids are higher than in a gas environment, the LIBS signal under equivalent laser excitation is significantly lower than in the presence of the sample–air interface.[14,15] Due to large energy losses in mechanical effects and in liquid evaporation, the plasma cools very rapidly. This produces a high rate of electron–ion recombination whose emission is continuum. An intense continuum emission is also present due to the Bremsstrahlung emission of the confined plasma, characterized by a high electron density.[9,14,16–22] After decay of the intense continuum emission in liquids, usually only the emission lines from low excitation levels emerge in SP LIBS. The spectral lines are strongly broadened due to the Stark effect and self-absorption in dense plasma. Different papers report a very short plasma duration ($<$1–2 µs) and the optimized LIBS signal detection with a very narrow gate width, in the order of 100 ns.[14,15,20,23,24] The obtained SP LIBS spectra can be used for recognition of only main sample constituents. The poor spectral properties of the SP LIBS spectra could be improved by increasing the laser pulse duration, for example, from 20 to 150 ns, as reported by Sakka *et al.*[25–28] The same research group performed the spatially resolved LIBS signal detection after SP excitation using 100 ns long pulses.[20] By shifting the collection point away from the hot plasma core, they obtained well resolved analytical lines. The majority of the results regarding SP LIBS still focuses on the early stage of the plasma evolution ($<$1 µs) while the long lasting plasma emission reported recently in ref. 29 has been far less examined.

The present study is focused on different mechanical and optical phenomena of the SP laser induced breakdown (LIB) on the aluminium target in water, with special attention to the late stage of the plasma evolution. Several experimental techniques including fast photography, Schlieren, shadowgraphy and optical emission spectroscopy are used to obtain insights into the plasma formation and evolution, shockwave propagation, cavitation bubble dynamics, and plasma spectral emission.

2 Experimental

The experimental setup used in this study is shown schematically in Fig. 1. The plasma was generated using a Nd:YAG laser (Molectron MY34) operated at 1064 nm, with 20 ns pulse duration and a pulse energy of 40 mJ. The laser beam was focused perpendicular to the target plane by two quartz plano-convex lenses L1 (f_1 = 100 mm) and L2 (f_2 = 68 mm), where the second lens was mounted directly on the chamber wall. Under the optimized conditions, the focal plane of the focusing system was slightly below ($\sim$0.5 mm) the surface of a pure aluminium target (99.999%). The target was placed vertically inside a chamber filled with 700 ml of distilled water. The optical path length of the laser beam through water was $\sim$3 cm. The chamber was equipped with two quartz windows w1 and w2, used for the lateral observation of the plasma and the vapour bubble. The target was shifted by 1 mm after each laser shot. Considering the Beer–Lambert law and water absorption coefficient α = 0.072 cm^{-1}, the estimated laser energy delivered to the target surface was 60% of the incident laser energy.[30] Based on the crater diameter on the target surface (250 $\pm$ 25 µm), the estimated fluence within an error of 12% was about 45 J cm^{-2} (2.25 GW cm^{-2}). Water inside the chamber was periodically exchanged to avoid scattering on the particles produced by LA of the sample.

Fast plasma imaging was performed through the lateral window w1 by using a biconvex achromatic lens L3 (f_3 = 100 mm) and a photographic objective lens OL (focal length 75 mm) mounted with macrobellows on an iCCD camera (Andor Technology, model DH734I-18U-03). The optical magnification of the system was determined using a reference object and the dispersion (0.01176 mm per px) was calculated for subsequent recordings.
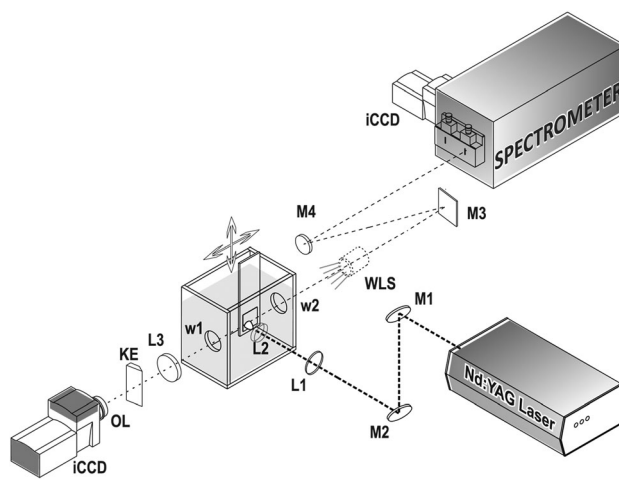

Fig. 1 Experimental setup: L1–L3 = lenses, M1, M2, and M3 = flat mirror, M4 = concave mirror, WLS = white light source, KE = knife edge, OL = objective lens, and w1 and w2 = quartz windows.

The iCCD was controlled using a pulse generator (DG-535, Stanford Research Systems), triggered optically by a fast photodiode that captures the laser beam partially reflected on mirror M2. The same optical setup was also used for shadowgraphy adding illumination using a white light source (WLS). The light from the WLS was guided by a fiber bundle (diameter 6 mm) to the chamber's lateral window w2. The same setup was used for the Schlieren imaging, where a vertically mounted knife-edge KE was positioned in the focus of lens L3, thus monitoring the refractive index gradient perpendicular to the sample. Images of the plasma were accumulated over 5 laser shots, except for long delays (>80 μs from the laser pulse) where 10 pulses were used; the acquisition gate width was varied between 15 ns and 50 μs. For shadowgraphs and Schlieren images only one laser pulse was applied and the gate width was varied between 20 ns and 2 μs.

For spectroscopic measurements the 1:1 image of the plasma plume was projected, by means of optical mirrors M3 and M4, on the entrance slit (100 μm wide) of a 0.5 m Ebert-type spectrometer equipped with a grating of 1180 grooves per mm. The iCCD detector was mounted at the spectrometer's exit plane and operated in an imaging mode. The spectra were reconstructed by manual binning of the pixels with the useful signal. All LIBS spectra were accumulated over 160 laser pulses, each one delivered to a fresh spot on the target.

3 Results and discussion

The dimension and shape of the laser induced plasma on the aluminium target inside water were studied by fast photography. Examples of plasma evolution at different delays after the laser pulse are shown in Fig. 2. From the photographs it is evident that during the first microsecond after the laser pulse the plasma is very bright and small, being confined by the surrounding liquid; in this phase, the detected plasma diameter does not exceed 400 μm. At about 400 ns from the laser pulse the plasma expansion perpendicular to the target slows down drastically; its further expansion occurs mostly in the direction parallel to the target surface. In this stage the plasma has a flat shape where its length parallel to the target is almost twice the height (direction normal to the target). The flat shape
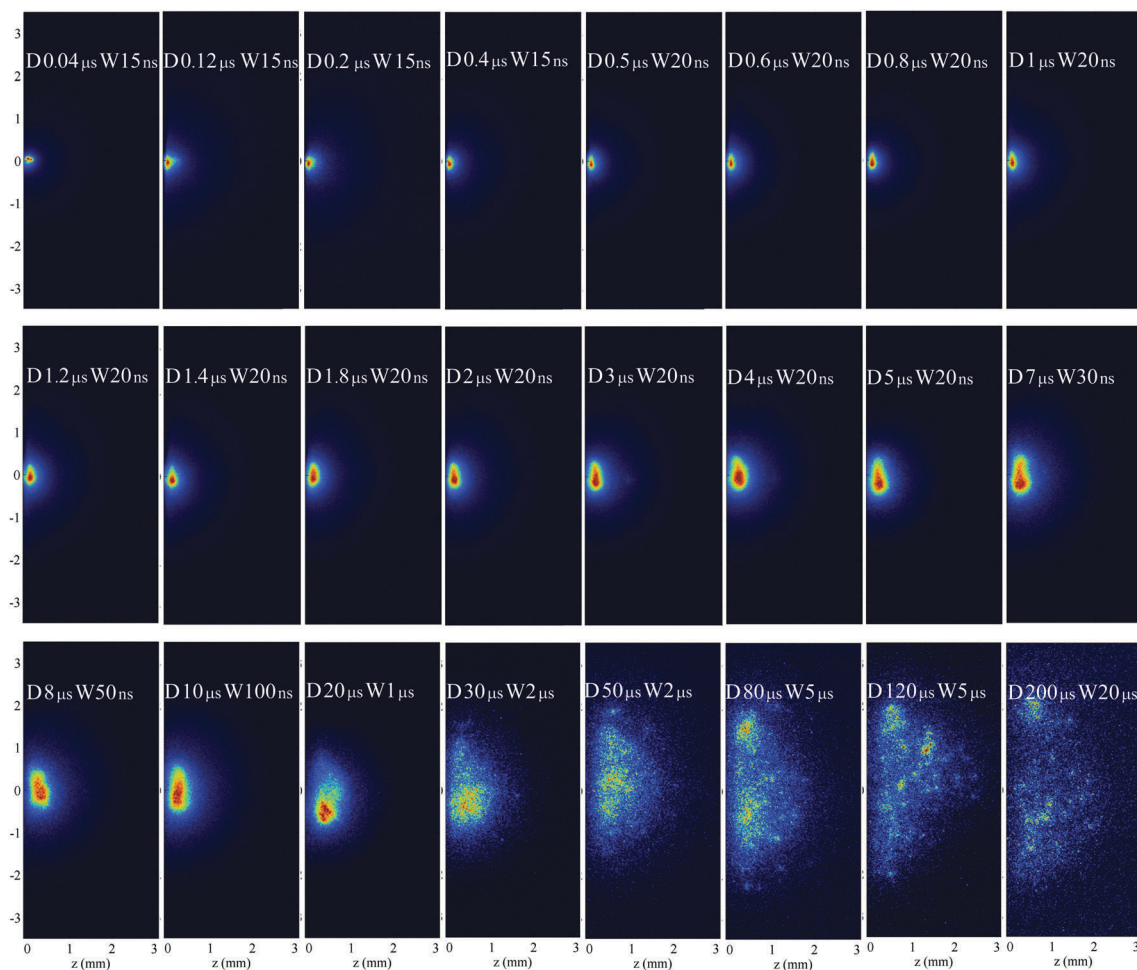

Fig. 2 Fast photography of the plasma evolving from the target (placed on the left) captured at different delays D from the laser pulse with acquisition gate width W.

of the plasma is visible until ∼10 μs; later it fulfils the growing vapour bubble and is characterized by the formation of glowing centres and their clustering. A flat plasma shape on submerged targets was observed by different authors,[25,31] but a long lasting emission (well beyond 1 μs) was reported only recently.[29] The typical duration of underwater plasma emission found in the literature is very short, in the order of a few hundreds of nanoseconds[22] or even shorter.[32] However, there are some studies that discuss about light emission on a longer timescale of a few microseconds. Lam et al.[33] gave a temporal dependence of the intensity of atomic Al lines and molecular AlO bands for a time period of 6 μs after the laser pulse. Although in ref. 33 the plasma plume formation and shape were not imaged, the experimental data clearly demonstrate that some emission still exists after several microseconds from the laser pulse. In ref. 25 a visible plasma emission was documented up to delays of 1000 ns and 2000 ns, for laser pulse durations of 20 ns and 100 ns, respectively. To date, a long lasting plasma emission after a SP laser excitation underwater was reported only by Lazic et al.,[29] where the plasma plume was detected up to 30 μs from the laser pulse. There, the plasma flattening was also observed and the authors identified two distinct plasma stages. The first stage, lasting for about 1 μs, is characterized by the rapidly expanding plume and by ejection of macroscopic hot particles from the sample surface; at the end of this phase the plasma emission almost disappears. In the second phase, the newly forming plasma expands slowly and smoothly from the target into the growing vapour bubble. This secondary plasma formation was explained by complex interaction of the hot plasma front with the surrounding which leads to the propagation of a high temperature and high pressure region back to the target. Similar phenomena were reported for LA in air[34,35] where a newly formed emissive plume detected at 3 μs after the laser pulse was attributed to the expulsion of the material by the backward reheated and melted sample layer. Slow target evaporation through the backward reheated target into the growing bubble was recently explained in the context of material removal during

LA in liquids.[30] This particular phase of LA is not always observed and it depends on the experimental conditions.

Starting from the plasma photographs (Fig. 2), for each acquisition delay the integral plasma intensity was calculated by summing the pixel intensities over the same area and subtracting the mean value over the dark region. The obtained values were then normalized on the gate width, the number of accumulations and on the nominal signal intensity as a function of the applied iCCD gain. The influence of the iCCD gain on the signal intensity was derived from measurements using an external light source. The normalized integral plasma intensity as a function of the acquisition delay is shown in Fig. 3, left. The plasma emission decays rapidly during the first 100 ns, as already reported in the literature.[36] However, at a delay of 500 ns we observed a sharp increase of the total plume intensity, coincident with the change in the plasma shape (see Fig. 2). At this point the plasma is well localized and enlarged on the target, thus producing efficient heating and additional material evaporation. In Fig. 3, right, the position of the maximum intensity plasma region above the target is shown as a function of time. After the initial fast forward movement of the most luminous plasma region (up to 250 μm from the target), the same moves back to the target after less than 100 ns. This is visible in the inset of Fig. 3, right. Similar phenomena were previously observed in the laser ablation of targets in air.[34,35] Other mechanisms driving this "backward motion" of the intense plasma emission towards the target (formation of the cavitation bubble, rebound of the internal shockwave, etc.) are also possible and should be further investigated. Successively, the position of the most intense emission region remains almost constant for a few microseconds and it is situated up to 200 μm from the target, Fig. 3, right. This high intensity, well localized and stable plasma over a few microseconds can be analysed using OES techniques using a large number of accumulations and larger gate widths with respect to the initial, fast decaying emission. In contrast to our results, some papers[20,25,37] reported the plasma images with a dark region immediately above the target; simultaneously, the
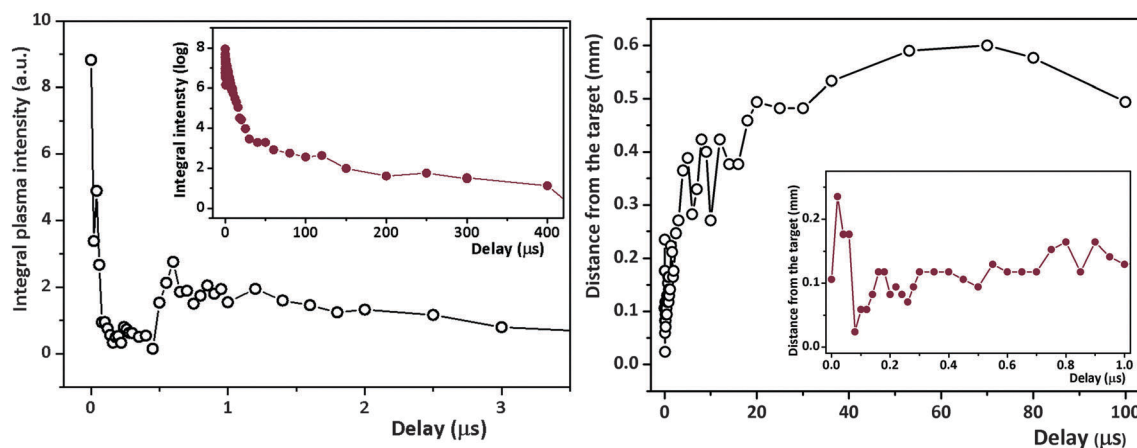

Fig. 3 Left: temporal dependence of integral plasma intensity for early delays (main figure) and later delays (inset). Right: the position of the maximum intensity plasma region with respect to the target for later delays (main figure) and early delays (inset).
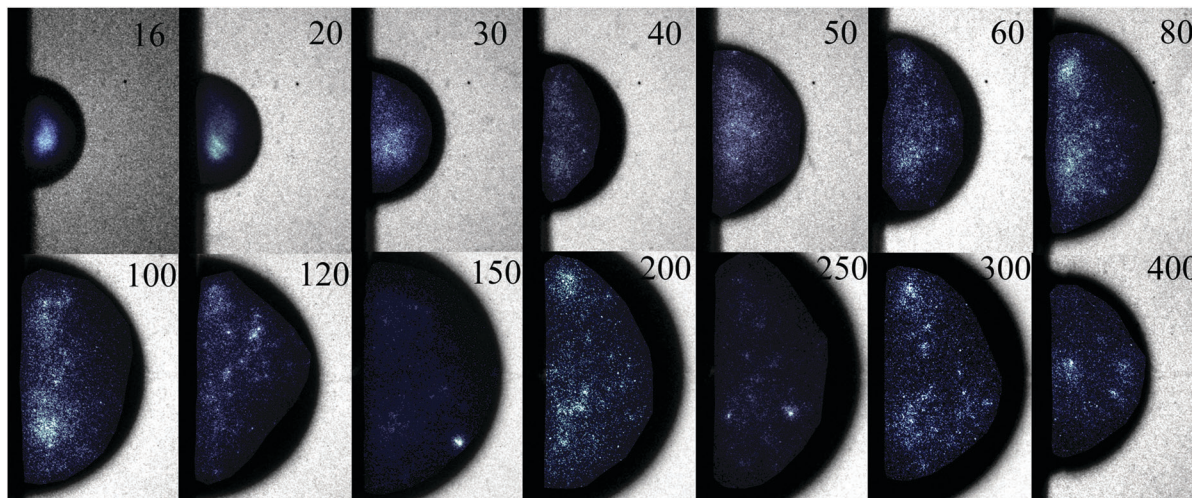
Fig. 4 Superimposed images of plasma photography (false colour) and shadowgraphy. Respective delays are shown in each photograph. Gate widths for shadowgraph measurements are 0.5 µs for 20 µs delay, 1 µs for 20−80 µs delays, and 2 µs for later delays. Gate widths for plasma photography are the same as those in Fig. 2.

plasma lifetime was very short (in the order of 100 ns), probably due to a lack of the backward heating of the target under the specific experimental conditions.

To our knowledge, this is the first time that a long lasting (over 100 µs) plasma emission was reported after single pulse laser ablation of a submerged target. Actually, some optically active species persist during the whole bubble cycle *i.e.* until its first collapse. The coexistence of light emitting centres and vapour bubble was checked using superimposed images obtained by fast photography and shadowgraphy, recorded using the same imaging system, and the results are shown in Fig. 4. Here, it seems that the plasma confinement inside the vapour bubble favours the long lasting optical emission, since no emitting centres were observed outside the cavity wall.

These results are in line with the recent research on the position and the origin of nanoparticles (NPs) in underwater ablation, claiming that all NPs are trapped inside the cavitation bubble.[32,38,39] The presence of the luminous emitting centres, tending to aggregate in the well expanded bubble (Fig. 4), indicates that the materials trapped inside the cavity hold temperature high enough to emit detectable light during the first evolution cycle. This conjecture is further justified by temperature measurements with the AlO molecular band up to a delay of 10 µs that clearly shows that the early bubble holds temperatures as high as 3500 K under our experimental conditions. Temperatures were evaluated using the program for AlO synthetic spectrum generation[40] and the example is shown in Fig. 5. These temperatures agree with the values reported by Casavola *et al.*[41] obtained by modelling of the bubble dynamics. If we adopt again the temperature values from the model[41] at the full bubble expansion $T \approx 1000$ K, this late emission can be ascribed to the blackbody radiation which can be detected using the employed system up to 850 nm. On the other hand it can be a weak emission from Na vapour which has a low temperature of evaporation (~ 1156.090 K) and a low lying excited level (16 973, 16 956 cm^{-1}) and is the longest observable
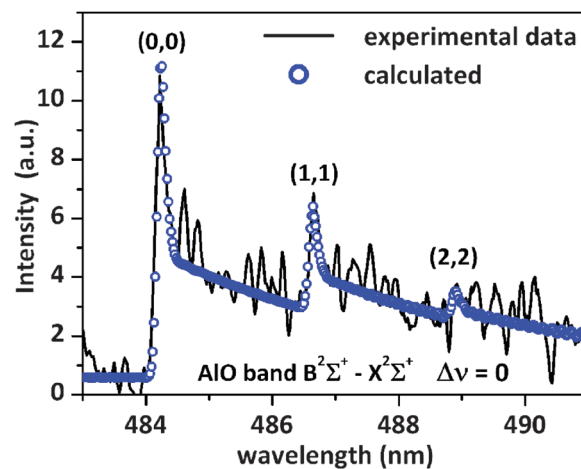

Fig. 5 Example of temperature evaluation by comparison of calculated and recorded AlO bands at a delay of 10 µs with 100 µs gate width.

line in the spectrum, up to 20 µs. A deeper understanding of the nature of these glowing centres requires further studies.

Extension of the bubble and the plasma emission at different delays from the laser pulse, measured along the target by shadowgraphy and photography, are shown in Fig. 6. At the beginning, their extension is similar but later, when the bubble is well expanded, the optical emitting region in photographs appears to be smaller than the bubble. We attribute this to an optical effect because the expanded vapour cavity has a lower refractive index than the surrounding water and behaves as a negative lens.[29,42] Rays originating near the bubble edge and travelling parallel to the axis of the collecting lens are deviated strongly by the expanded and cooled bubble, so that they do not reach the detector, thus creating the image of a dark layer close to the bubble wall.

From Fig. 4, it is found that the maximum bubble expansion occurs 260 µs after the laser pulse, and its radius is ~ 3.157 mm
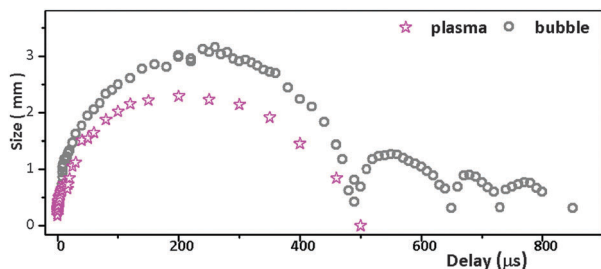
Fig. 6 The plasma and the bubble radius at the target plane, determined from photographs.

and ~3.371 mm in the direction parallel and normal to the target surface, respectively. The bubble remains slightly elongated towards the laser source during the expansion. Differently, in the shrinking phase a part of the bubble just above the target starts to deform, increasing the contact angle, as evident in Fig. 4 at a delay of 400 μs. Similar phenomena were also observed by Ibrahimkutty et al.,[43] who speculated that still high surface temperature can be responsible for the observed change in the contact angle between vapour, liquids and solids.

In our experiment, the bubble collapses after about 475 μs from the laser pulse. Based on the experimentally determined radius and collapse time of the bubble, the energy contained in the bubble was estimated using formula (1) widely used in the literature:[3,44]

$$E_b = V(p_{stat} - p_v) \qquad (1)$$

where V denotes the bubble volume. The difference between static pressure in liquid and pressure of the vapour inside the bubble ($p_{stat} - p_v$) is inferred using (2)

$$T_b = 2 \cdot 0.915 \cdot R_{max} \sqrt{\frac{\rho}{p_{stat} - p_v}} \qquad (2)$$

where T_b represents the bubble oscillation period[27,45] i.e. time elapsed between bubble formation and the collapse. The time of the bubble collapse was determined from the Schlieren images based on the release of the second shock wave upon the bubble collapse, Fig. 7 – last two images in the sequence. Eqn (2) was derived for spherical bubbles but has already been proven to be applicable for elongated bubbles,[27] as is the case here. R_{max} for elongated bubbles corresponds to the radius of a sphere which has the same volume as the elongated bubble.[44] In this way the energy stored in the bubble was calculated to be 10.8 mJ. Three bubble rebounds were detected after the initial collapse, which lasted up to 900 μs after the laser pulse.
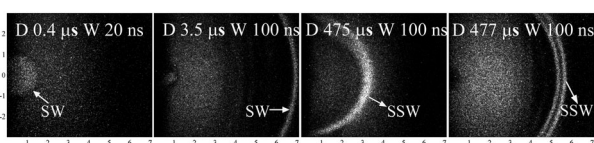

Fig. 7 Images of the shock wave obtained using the Schlieren technique, at different delays D from the laser pulse; W is the acquisition gate width.

During the successive rebounds the bubble had less regular shape and it was flattened on the target.

From the measured position of the outer SW front, the initial velocity of the SW is 3 km s^{-1} at 100 ns; after 1 μs it decreases to 1.6 km s^{-1}. The peak pressure as a function of a SW velocity can be obtained using the equation found in the literature.[11,46] For our experimental conditions derived values of pressure are 2.29 GPa at the earlier delays and 86 MPa after 1 μs, similar to those reported in the literature.[32] The velocity of the second SW could not be determined using the employed measurement procedure due to slight fluctuations in the time of the bubble collapse and the subsequent release of the second SW (±2 μs).

We return now from mechanical effects to optical emission which is of primary interest from the standpoint of LIBS. From the LIBS spectra acquired at different delays from the laser pulse, analogous to the results related to Fig. 2, we observed two distinct phases of plasma evolution. The first phase is dominated by an intense continuum emission that is a direct consequence of a large electron density. This phase lasts shortly, up to a delay of 500 ns from the laser pulse. Here, the resonant lines of aluminium $3s^23p–3s^24s$ ($^2P^0–^2S$) and sodium $2p^63s–2p^63p$ ($^2S–^2P^0$) impurities were detected; these lines were highly broadened and almost masked by the continuum emission. Beside the atomic lines, molecular AlO bands $(0,0)$ $B^2\Sigma^+ \rightarrow X^2\Sigma^+$ were detected already at 100 ns after the laser pulse. Appearance of the molecular bands so early in the plasma is characteristic of rapidly cooling underwater plasmas.[11] Furthermore, due to an efficient dissociation of water molecules which produces abundance of oxygen atoms in the plasma, the oxidation rate of the target material is high leading to the formation of AlO species. The same molecular emission during underwater LA of alumina was recently reported by Lam et al.[33]

After 500 ns from the laser pulse, the plasma continuum radiation almost completely vanishes but the emission from low lying levels of atoms and molecules is still present (Fig. 8a). A further increase of the acquisition delay up to 2 μs leads to a new growth in the analytical signal (Fig. 8b). Comparing the spectra obtained at delays of 0.5 μs and 2 μs, in the second case there is a significant improvement in signal strengths and the quality of the lines. By setting the gate width to 100 μs at a delay of 5 μs clearly resolved spectra with further improvement in the signal to noise ratio are obtained (Fig. 8c). The longest lasting emission is detected from Na atoms, probably due to the lowest energy of the excited level. Weak Na emission was detected even at delays of 20 μs. This result is quite comparable with the emission duration in the gas surrounding.[47–49]

Evolution of the peak line intensities after the background subtraction, and the corresponding signal-to-noise ratios (SNR) are depicted in Fig. 9. The delay times before 0.5 μs are omitted here due to a preponderant continuum contribution. Although different lines have peak emission intensity at different delays, from Fig. 9a it can be seen that the most intense emission is delayed by 1–2 μs with respect to the laser pulse for all of them. This late LIBS signal increase is especially pronounced for the molecular AlO species, which are optimally emitted when the
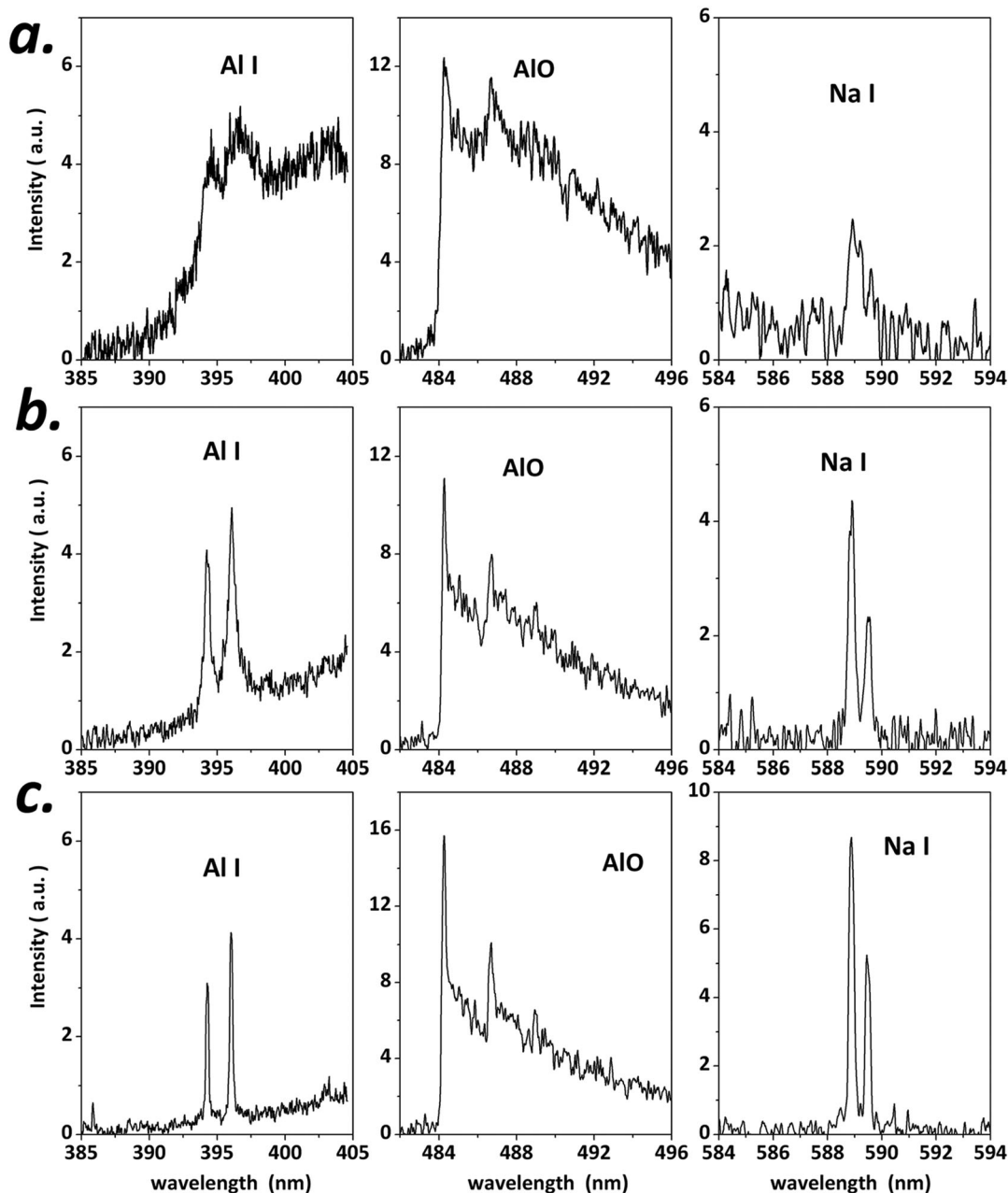
Fig. 8 Spectra obtained using SP LIBS on the aluminium target underwater with 160 accumulations: (a) delay: 0.5 μs and gate width: 0.5 μs, (b) delay: 2 μs and gate width: 0.5 μs and (c) delay: 5 μs and gate width: 100 μs.

temperature is between 3500 and 4000 K, because AlO radicals dissociate into atoms at higher temperatures and form into polyatomic aggregates at lower temperatures.[50] The signal quality in terms of SNR importantly increases for longer delays (Fig. 9b). For the molecular species the maximum SNR, measured with a gate width of 0.5 μs, occurs 2 μs after the laser pulse, while the atomic transitions show a steady increase of SNR up to 4 μs. The line intensity evolution for delays up to 10 μs, measured with a gate width of 100 μs, is shown in Fig. 9c, and the corresponding SNR is given in Fig. 9d. Increasing the gate width during the secondary plasma evolution leads to a manifold increase in the SNR with respect to the detection of the early plasma with short

acquisition gates often used in the LIBS experiments.[14,15,20,23,24] The corresponding emission lines are well resolved and almost free from the continuum background, as evident from Fig. 8c.

Based on the FWHM of recorded lines and on the low continuum component, it is clear that secondary plasma has much lower electron density than the initial plume formed immediately after the laser pulse. In the secondary plasma phase there are no violent material expulsion, and no abrupt changes in pressure, temperature and shape. In this phase, the vapour bubble is already formed, and its presence seems to increase the secondary plasma persistence, as in the case of double pulse LIBS.[3,14,23] The just formed bubble is small, so
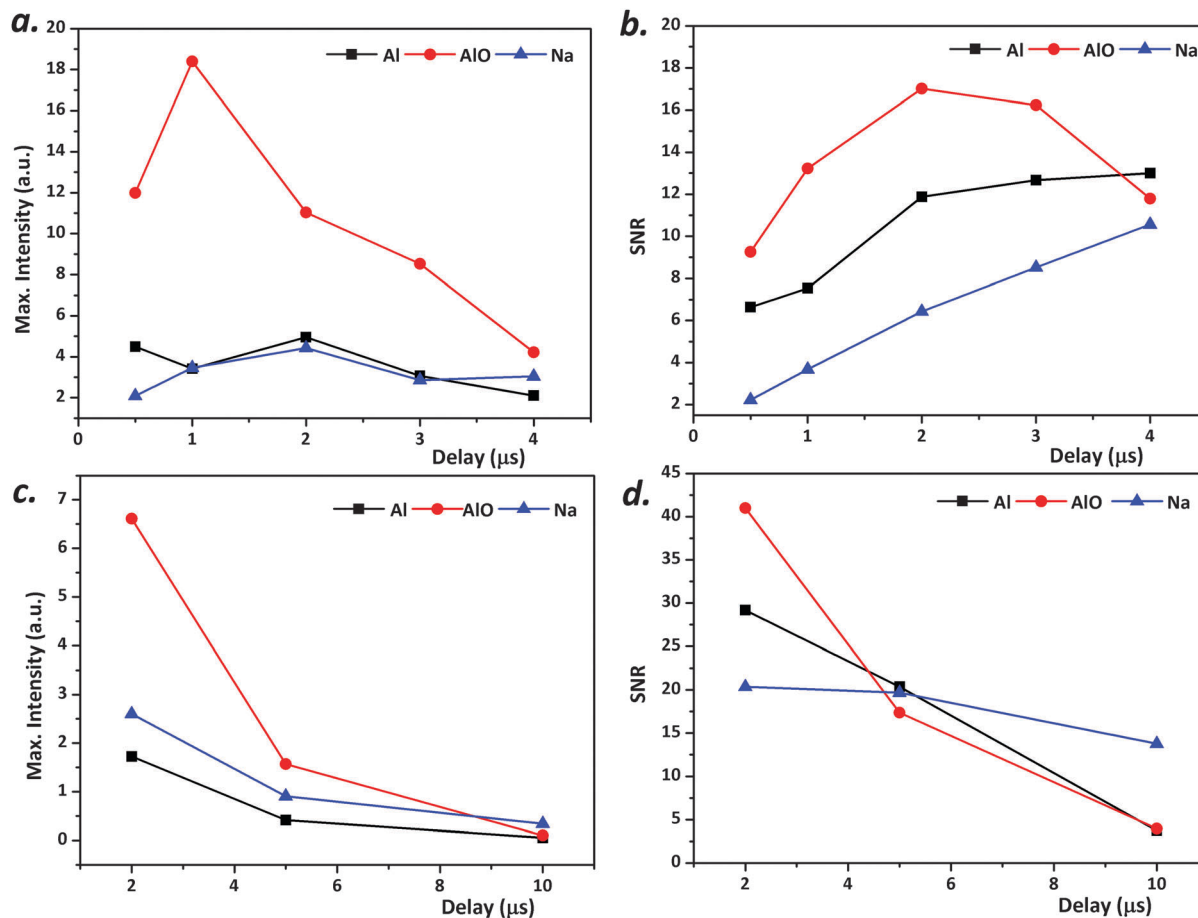
This journal is © the Owner Societies 2016

Phys. Chem. Chem. Phys., 2016, **18**, 14629–14637 | **14635**

Fig. 9   Intensity and SNR evolution of different excited species during SP LIBS on the pure Al target underwater: (a and b) gate width: 0.5 μs; (c and d) gate width: 100 μs.

there is a limited heat exchange across its interface with the surrounding liquid interface. The plasma expansion is also limited by the bubble wall and remains well localized during the first tens of microseconds. Later, due to a large bubble expansion, the confined plasma no longer holds high pressure and temperature, and hence the emission from the excited states of atoms and molecules progressively disappears. The disappearance of the LIBS signal also occurs due to the movement of the maximum intensity region away from the target (Fig. 3, right), so that it is not focused efficiently onto the entrance slit of the spectrometer.

4 Conclusions

The results of the spatial and temporal studies of the plasma formed after single pulse laser ablation of the aluminium target underwater performed using different optical techniques are presented here.

The obtained results show that it is possible to produce long lasting plasma underwater by applying single pulse laser ablation. Here detected plasma has two characteristic evolution phases. In the first stage, immediately after the laser pulse and with a duration of less than 500 ns, the plasma rapidly expands and decays, where the optical emission is characterized by an intense continuum component and very large widths of the detected lines. Here, the

LIBS signal has a poor quality in terms of the spectral resolution and signal-to-noise ratio. The successive plasma phase starts from the backward reheated target. Its emission has a stable position close to the target and still growing intensity over tens of microseconds from the laser pulse. Later optical emission, detected over the whole bubble cycle, remains confined inside the expanded vapour cavity. The secondary plasma has significantly lower electron densities with respect to the first plasma stage, and hence it is almost free from the continuum component.

Here, we demonstrated that well resolved and intense spectral lines can be obtained by single pulse laser excitation if avoiding the initial phase of the plasma evolution (approximately during the first 500 ns), and by using large acquisition gate widths, in the order of 10–100 μs. These findings are very important for performing LIBS measurements inside a liquid environment, since a good analytical signal can be obtained by using a single, commercial laser source.

Acknowledgements

References

1 T. Kovalchuk, G. Toker, V. Bulatov and I. Schechter, *Chem. Phys. Lett.*, 2010, **500**, 242.

2 A. V. Simakin, V. V. Voronov and G. A. Shafeev, *Phys. Wave Phenom.*, 2007, **15**, 218.

3 G. Cristoforetti, M. Tiberi, A. Simonelli, P. Marsili and F. Giammanco, *Appl. Opt.*, 2012, **51**, B30.

4 V. Lazic, F. Colao, R. Fantoni, V. Spizzichino and S. Jovićević, *Spectrochim. Acta, Part B*, 2007, **62**, 30.

5 T. T. P. Nguyen, R. Tanabe and Y. Ito, *Appl. Phys. Express*, 2013, **6**, 122701.

6 V. Lazic, LIBS analysis of liquids and of materials inside liquids, in *Laser Induced Breakdown Spectroscopy: Theory and Applications*, ed. S. Mussazzi and U. Perini, Springer & Verlag, 2014.

7 A. Vogel, J. Noack, K. Nahen, D. Theisen, S. Busch, U. Parlitz, D. X. Hammer, G. D. Noojin, B. A. Rockwell and R. Birngruber, *Appl. Phys. B: Lasers Opt.*, 1999, **68**, 271.

8 J. Noack, D. X. Hammer, G. D. Noojin, B. A. Rockwell and A. Vogel, *J. Appl. Phys.*, 1998, **83**, 7488.

9 A. De Giacomo, M. Dell'Aglio, R. Gaudiuso, S. Amoruso and O. De Pascale, *Spectrochim. Acta, Part B*, 2012, **78**, 1.

10 N. Takada, T. Nakano and K. Sasaki, *Appl. Phys. A: Mater. Sci. Process.*, 2010, **101**, 255.

11 P. K. Kennedy, D. X. Hammer and B. A. Rockwell, *Prog. Quantum Electron.*, 1997, **21**, 155.

12 I. Akhatov, O. Lindau, A. Topolnikov, R. Mettin, N. Vakhitova and W. Lauterborn, *Phys. Fluids*, 2001, **13**, 2805.

13 H. W. Kang, H. Lee and A. Welch, *J. Appl. Phys.*, 2008, **103**, 083101.

14 A. De Giacomo, M. Dell'Aglio, O. De Pascale and M. Capitelli, *Spectrochim. Acta, Part B*, 2007, **62**, 721.

15 A. De Giacomo, M. Dell'Aglio, F. Colao, R. Fantoni and V. Lazic, *Appl. Surf. Sci.*, 2005, **247**, 157.

16 K. Sasaki and N. Takada, *Pure Appl. Chem.*, 2010, **82**, 1317.

17 B. Kumar, D. Yadav and R. K. Thareja, *J. Appl. Phys.*, 2011, **110**, 074903.

18 K. Saito, K. Takatani, T. Sakka and Y. H. Ogata, *Appl. Surf. Sci.*, 2002, **197–198**, 56.

19 A. De Giacomo, M. Dell'Aglio and O. De Pascale, *Appl. Phys. A: Mater. Sci. Process.*, 2004, **79**, 1035.

20 A. Matsumoto, A. Tamura, K. Fukami, Y. H. Ogata and T. Sakka, *Anal. Chem.*, 2013, **85**, 3807.

21 V. Amendola and M. Meneghetti, *Phys. Chem. Chem. Phys.*, 2013, **15**, 3027.

22 M. Dell'Aglio, R. Gaudiusoa, O. De Pascalea and A. De Giacomo, *Appl. Surf. Sci.*, 2015, **348**, 4.

23 A. De Giacomo, M. Dell'Aglioa, F. Colao and R. Fantoni, *Spectrochim. Acta, Part B*, 2004, **59**, 1431.

24 H. Suzuki, H. Nishikawa and I.-Y. Sandy Lee, *PhysChemComm*, 2002, **5**, 88.

25 H. Oguchi, T. Sakka and Y. H. Ogata, *J. Appl. Phys.*, 2007, **102**, 023306.

26 T. Sakka, S. Masai, K. Fukami and Y. H. Ogata, *Spectrochim. Acta, Part B*, 2009, **64**, 981.

27 B. Thornton, T. Sakka, T. Takahashi, A. Tamura, T. Masamura and A. Matsumoto, *Appl. Phys. Express*, 2013, **6**, 08240.

28 T. Sakka, H. Oguchi, S. Masai, K. Hirata and Y. H. Ogata, *Appl. Phys. Lett.*, 2006, **88**, 061120.

29 V. Lazic, J. J. Laserna and S. Jovicevic, *Spectrochim. Acta, Part B*, 2013, **82**, 42.

30 V. Lazic and S. Jovićević, *Spectrochim. Acta, Part B*, 2014, **101**, 288.

31 B. Thornton and T. Ura, *Appl. Phys. Express*, 2011, **4**, 022702.

32 T. Tsuji, Y. Okazaki, Y. I. Tsuboi and M. Tsuji, *Jpn. J. Appl. Phys.*, 2007, **46**, 1533.

33 J. Lam, D. Amans, F. Chaput, M. Diouf, G. Ledoux, N. Mary, K. Masenelli Varlot, V. Motto Ros and C. Dujardin, *Phys. Chem. Chem. Phys.*, 2014, **16**, 963.

34 Y. Zhou, S. Tao and B. Wu, *Appl. Phys. Lett.*, 2011, **99**, 051106.

35 S. Tao, Y. Zhou, B. Wu and Y. Gao, *Appl. Surf. Sci.*, 2012, **258**, 7766.

36 A. De Giacomo, M. Dell'Aglio, A. Santagata, R. Gaudiuso, O. De Pascale, P. Wagener, G. C. Messina, G. Compagninie and S. Barcikowski, *Phys. Chem. Chem. Phys.*, 2013, **15**, 3083.

37 A. Matsumoto, A. Tamura, K. Fukami, Y. H. Ogata and T. Sakka, *J. Appl. Phys.*, 2013, **113**, 053302.

38 P. Wagener, S. Ibrahimkutty, A. Menzel, A. Plech and S. Barcikowski, *Phys. Chem. Chem. Phys.*, 2013, **15**, 3068.

39 W. Soliman, N. Takada and K. Sasaki, *Appl. Phys. Express*, 2010, **3**, 035201.

40 C. G. Parigger, A. C. Woods, D. M. Surmick, G. Gautama, M. J. Witte and J. O. Hornkohl, *Spectrochim. Acta, Part B*, 2015, **107**, 132.

41 A. Casavola, A. De Giacomo, M. Dell'Aglio, F. Taccogna, G. Colonna, O. De Pascale and S. Longo, *Spectrochim. Acta, Part B*, 2005, **60**, 975.

42 V. Lazic, S. Jovićević and M. Carpanese, *Appl. Phys. Lett.*, 2012, **101**, 054101.

43 S. Ibrahimkutty, P. Wagener, T. dos S. Rolo, D. Karpov, A. Menzel, T. Baumbach, S. Barcikowski and A. Plech, *Sci. Rep.*, 2015, **5**, 16313.

44 K. Sasaki, T. Nakano, W. Soliman and N. Takada, *Appl. Phys. Express*, 2009, **2**, 046501.

45 J.-P. Franc and J.-M. Michel, Fundamentals of Cavitation, in *Fluid Mechanics And Its Applications*, ed. R. Moreau, Kluwer Academic Publishers, 2004, vol. 76, p. 38.

46 W. Lauterborn and A. Vogel, ShockWave Emission by Laser Generated Bubbles, in *Bubble Dynamics and Shock Waves*, ed. C. F. Delale, Springer Berlin Heidelberg, 2013, p. 75.

47 M. Capitelli, G. Colonna, G. D'Ammando, R. Gaudiuso and L. D. Pietanza, Physical Processes in Optical Emission Spectroscopy, in *Laser Induced Breakdown Spectroscopy: Theory and Applications*, ed. S. Mussazzi and U. Perini, Springer & Verlag, 2014.

48 D. A. Cremers and L. J. Radziemski, *Handbook of Laser-Induced Breakdown Spectroscopy*, John Wiley & Sons Ltd, 2006.

49 R. Noll, *Laser-Induced Breakdown Spectroscopy: Fundamentals and Applications*, Springer, Berlin, 2012.

50 P. W. J. M. Boumans, *Theory of Spectrochemical Excitation*, Springer, US, 1995, p. 145.

Effects of a Preembedded Axial Magnetic Field on the Current Distribution in a Z-Pinch Implosion

D. Mikitchuk,[1,*] M. Cvejić,[1] R. Doron,[1] E. Kroupp,[1] C. Stollberg,[1] Y. Maron,[1] A. L. Velikovich,[2]
N. D. Ouart,[2] J. L. Giuliani,[2] T. A. Mehlhorn,[2] E. P. Yu,[3] and A. Fruchtman[4]

[1]*Weizmann Institute of Science, Rehovot 76100, Israel*
[2]*Plasma Physics Division, Naval Research Laboratory, Washington, DC 20375, USA*
[3]*Sandia National Laboratories, P.O. Box 5800, Albuquerque, New Mexico 87185-1186, USA*
[4]*Holon Institute of Technology, P.O. Box 305, Holon 58102, Israel*

The fundamental physics of the magnetic field distribution in a plasma implosion with a preembedded magnetic field is investigated within a gas-puff Z pinch. Time and space resolved spectroscopy of the polarized Zeeman effect, applied for the first time, reveals the impact of a preembedded axial field on the evolution of the current distribution driven by a pulsed-power generator. The measurements show that the azimuthal magnetic field in the imploding plasma, even in the presence of a weak axial magnetic field, is substantially smaller than expected from the ratio of the driving current to the plasma radius. Much of the current flows at large radii through a slowly imploding, low-density plasma. Previously unpredicted observations in higher-power imploding-magnetized-plasma experiments, including recent, unexplained structures observed in the magnetized liner inertial fusion experiment, may be explained by the present discovery. The development of a force-free current configuration is suggested to explain this phenomenon.

Compression of magnetic flux and magnetized plasma is a fundamental problem manifested in a variety of conducting fluid phenomena in laboratory plasmas and astrophysics [1–5]. Recently, this subject has gained particular interest due to the advances in producing plasmas of high temperature and density for fusion purposes, based on the approach of magnetized plasma compression [3,6]. These advances follow three decades of experimental [7–14] and theoretical [15,16] research. Some of the magnetized-plasma implosion experiments [7,8,11,17–19] reveal new and unpredicted phenomena, yet to be fully understood, which dramatically differ from those observed in implosion experiments without a preembedded axial magnetic field. These include significant changes in the plasma dynamics and radiation emission properties, specifically, (i) the formation of helical structures [17,18], (ii) larger than predicted implosion time and plasma radius at stagnation [18,19] accompanied by strong mitigation of instabilities [11,18], and (iii) reduction of the continuum [7,8] and K-shell emission [11]. In order to advance the concept of magnetized plasma compression, it is essential to understand the governing mechanisms of these phenomena.

A key parameter for the understanding of the physics occurring during the implosion and at stagnation is the compressing azimuthal magnetic field (B_θ). Knowledge of the magnetic field is required for inferring the current distribution, the magnetic field diffusion, the energy balance, and for comparisons with simulations. However,

reliable experimental data on the B-field distribution in Z pinches are scarce due to the high electron densities, high ion velocities, and transient nature of the plasma, which make measurements of B fields in such plasmas rather difficult. We note a few examples of such spectroscopic measurements in gas-puff Z pinches [20–22], and measurements based on Faraday rotation in wire-array Z pinches [23].

Here, we present an experimental determination of B_θ throughout the magnetized plasma implosion, achieved using a noninvasive spectroscopic technique that provides a high sensitivity for the Zeeman effect [24]. This technique is based on the polarization properties of the Zeeman components for light emission viewed parallel to the B field, as described in Refs. [25–28], and recently implemented for Z-pinch implosions [22]. These measurements showed that the application of an initial axial magnetic field (B_{z0}) has a significant effect on the current distribution in the plasma: a large part of the current does not flow in the imploding plasma, rather it flows through a low-density plasma (LDP) residing at large radii (here, by "current distribution" we mean the partition of the total current between the flow in the imploding plasma and the LDP). We believe that these findings are of general nature and can explain various unexplained phenomena mentioned above.

We note that previous measurements in classical Z pinches have indicated that during the stagnation some of the current is carried by an imploding trailing plasma [23,29].
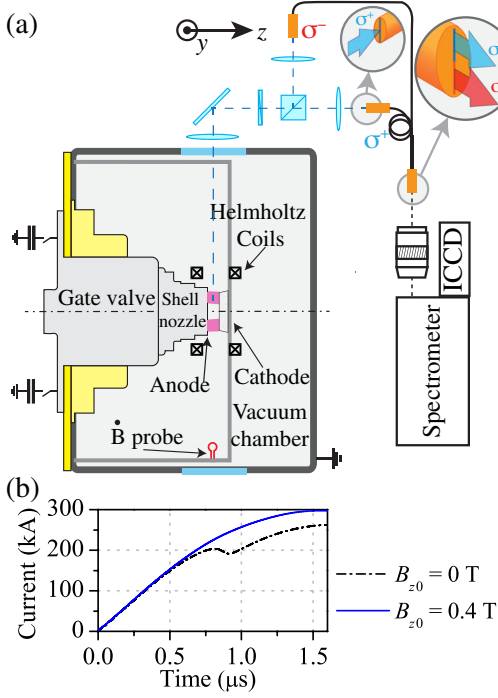
(a)

(b)

FIG. 1.   (a) Schematic description of the experimental setup and spectroscopic system used for B_θ measurements. (b) Shot-averaged current traces obtained with a B-dot probe ($z = 5$ mm, $r = 120$ mm) for different values of B_{z0} (more details are given in the Supplemental Material [30]).

FIG. 2.   (a) Spectral image of the Ar III $4s - 4p$ transition ($\lambda = 3301.85$ Å), for $B_{z0} = 0$. (b) Spectral line shapes of the σ^+ (blue circles) and σ^- (red squares) Zeeman components along with the best fits (blue solid and red dashed lines). (c) Spectral image for $B_{z0} = 0.4$ T. (d) Explanations are the same as in (b). y is the distance of the chord to the axis. The dashed white vertical line in (a) and (c) represents the unshifted position of the line center ($B_\theta = 0$). The horizontal lines mark the lineout positions.

However, here we show a completely different phenomenon that is directly related to the presence of an applied B_z.

In our configuration [Fig. 1(a)], a cylindrical argon gas-puff shell (initial radius 19 mm and mass 30 μg/cm, as determined by interferometry), containing a preembedded, quasistatic axial magnetic flux ($B_{z0} \leq 0.4$ T), prefills the anode-cathode gap (10 mm). Subsequently, a pulsed current (rising to 300 kA in 1.6 μs) is driven through the gas, ionizes it, and generates an azimuthal magnetic field that compresses the plasma radially inward together with the embedded B_z field. B_{z0} is generated by a pair of Helmholtz coils (HC) carrying a long current pulse ($\sim$5 ms) to allow for the diffusion of B_{z0} into the anode-cathode gap.

As shown in Fig. 1(a), the imploding plasma column is radially observed. The collected light passes through a quarter-wave plate that transforms the circularly polarized σ^+ and σ^- components into orthogonal linear polarizations that are subsequently split using a polarizing beam splitter. Each of the two polarizations is then imaged on a separate linear array of 50 optical fibers. The two ends of the fiber arrays are imaged along the entrance slit of a high-resolution (0.3 Å), imaging spectrometer; its output coupled to a gated (10 ns) intensified charge-coupled device (ICCD). This setup allows for a simultaneous recording of the two polarization components, emitted from exactly the same plasma volume, on different parts of a single detector, with a spatial resolution of 0.3 mm in the radial and axial directions.
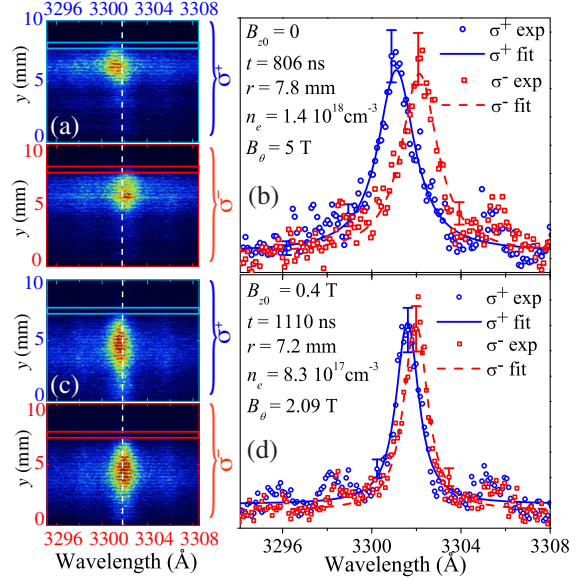
Here, for the determination of B_θ, we use the σ^+ and σ^- Zeeman components of the Ar III $(^4S)4s\,^5S_2 - (^4S)4p\,^5P_2$ transition ($\lambda = 3301.85$ Å). Figure 2(a) presents a typical spectral image obtained at $z = 5$ mm ($z = 0$ is the anode surface) and $t = 806$ ns ($t = 0$ is the beginning of the current pulse) for $B_{z0} = 0$. The upper and lower halves show the plasma emission of the σ^+ and σ^- components, respectively, chordally integrated along the line of sight. Figure 2(b) shows the line shapes of the σ^+ and σ^- Zeeman components, obtained from the spectral image [Fig. 2(a)] by integrating the data over $\Delta y = 0.3$ mm at the outermost y of the plasma, along with their best fits. r_{imp} is defined at 20% of the peak emission after inverse Abel transform of the Ar III line intensity distribution (the Ar III line is optically thin and 2D images confirm that the plasma posses cylindrical symmetry). For $\vec{B} = B_\theta\hat{\theta}$, using the emission from the outermost plasma radii ensures that the line of sight is parallel to $\vec{B}$. It was verified, using visible 2D imaging, that the outermost radii of the imploding plasma and of the Ar III emission coincide.

Since the Zeeman splitting within each of the σ components is small (≤ 0.025 Å for $B = 1$ T), each of the σ^+ and σ^- line shapes is fitted with a Voigt profile, where the Gaussian part accounts for instrumental and Doppler broadening, and the Lorentzian part is due to the Stark broadening. B_θ is then extracted from the wavelength difference between the peaks ($\Delta\lambda$) of the best fits [where
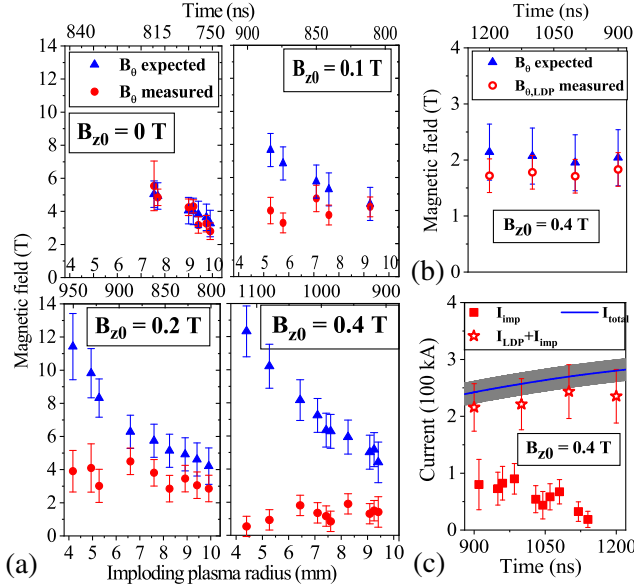
FIG. 3. (a) B_θ as a function of the outer imploding plasma radius, measured at $z = 3.5$ mm for $B_{z0} = 0, 0.1, 0.2,$ and 0.4 T, together with the B_θ expected, calculated using the total current. The upper scale shows the typical times that correspond to each plasma radius (times of stagnation for $B_{z0} = 0, 0.1, 0.2,$ and 0.4 T are 860 ± 20, 920 ± 20, 1030 ± 30, and 1160 ± 40 ns, respectively). (b) B_θ measured and B_θ expected as a function of time at the LDP outer radius ($r_{\text{out,LDP}} \sim 25$–27 mm) at $z = 3.5$ mm for $B_{z0} = 0.4$ T. (c) Currents inferred from B_θ measurements within the imploding plasma (red squares), I_{imp}, and within the LDP outer radius (red stars), $I_{\text{LDP}} + I_{\text{imp}}$, together with I_{total} (blue line) from the B-dot measurement, for $B_{z0} = 0.4$ T. Grey region around the I_{total} represents uncertainty in the total current measurement.

$B_\theta(\text{T}) = 5 \times \Delta\lambda(\text{Å})$ [24], for the Ar III line], and n_e is obtained from the Lorentzian width.

Figures 2(c) and 2(d) are the same as Figs. 2(a) and 2(b) but for $B_{z0} = 0.4$ T, obtained at $t = 1110$ ns. The spectral images in Fig. 2 are chosen such that, at the time of their recording, the outer plasma radius is similar ($r_{\text{imp}} \approx 7.8$ mm for $B_{z0} = 0$, and $r_{\text{imp}} \approx 7.2$ mm for $B_{z0} = 0.4$ T). For these conditions, and assuming the entire current is flowing through the imploding plasma, we expect that B_θ would be lower for the case of $B_{z0} = 0$, due to the significantly smaller current measured by the B-dot probe at the time of the spectra recording [$\sim$195 kA for $B_{z0} = 0$, $\sim$270 kA for $B_{z0} = 0.4$ T, as seen from Fig. 1(b)]. However, while the measured B_θ in the case of $B_{z0} = 0$ is $B_\theta \cong 5$ T, as expected, in the case of $B_{z0} = 0.4$ T, the measured $B_\theta \cong 2.1$ T is much lower than expected from Ampere's law. Considering the fact that, in implosions with axial B field, the total $\vec{B}$ might be not parallel to our line of sight, the calculations show that the true B_θ is even lower than 2.1 T.

Figure 3(a) shows the measurements of B_θ at the plasma outer radius for $B_{z0} = 0, 0.1, 0.2,$ and 0.4 T, together with B_θ expected, calculated by assuming the entire measured circuit current flows within the plasma radius ($B_\theta = \mu_0 I/2\pi r_{\text{imp}}$). We note that each data point is obtained from a separate shot, and that different sets of shots have shown that the results were reproducible to within the error bars indicated. For $B_{z0} = 0$, B_θ measured shows that the entire current flows within the imploding shell. On the other hand, for $B_{z0} > 0$, B_θ measured differs significantly from B_θ expected. This phenomenon is observed over the entire anode-cathode gap (see Supplemental Material [30]). This shows that the application of B_z significantly affects the current distribution in the plasma, such that only part of the current flows through the imploding plasma. Furthermore, it is seen that the fraction of the total current that flows in the imploding plasma decreases with B_{z0}. Additionally, Fig. 3(c) shows that for $B_{z0} = 0.4$ T the current within the imploding plasma drops with time. Before we discuss the implications of these measurements on the plasma dynamics, we first show that the missing current flows in a low-density plasma (LDP) residing at radii larger than that of the imploding plasma.

To this end, plasmas were searched for up to the vacuum chamber wall using 2D and spectral imaging (see Supplemental Material [30]). These measurements revealed the existence of plasma at $20 \lesssim r \lesssim 27$ mm, which consists of argon, carbon, and hydrogen ions ($10^{16} \lesssim n_e \lesssim 10^{17}$ cm^{-3} from Stark broadening, $T_e \sim 4$–6.5 eV from line intensities). B_θ measurements at the outer radius of this LDP, using Zeeman splitting of the C IV $3s - 3p$ transition ($\lambda = 5801$ Å) are presented in Fig. 3(b). It shows that the current flowing within $\lesssim 27$ mm accounts for nearly the entire current measured by the B dot [see Fig. 3(c)], providing a definite answer for the missing current in the imploding plasma.

It is emphasized that the LDP is also observed when $B_{z0} = 0$. However, its n_e and T_e remain low throughout the implosion ($n_e \lesssim 10^{16}$ cm^{-3}, $T_e \leq 2$ eV), consistent with the absence of current flow there. It is only in the presence of $B_{z0} > 0$ that the LDP carries a significant part of the current.

It can be further seen in Fig. 3 that the ratio of I_{LDP} to the imploding plasma current rises with time. This is explained by the rise of the imploding plasma impedance due to the increase of $d(LI)/dt$ and resistance (plasma cross section is decreasing, but its resistivity, inferred from T_e measurements, is nearly constant), whereas the LDP impedance remains almost constant [this explains the difference between the current traces shown in Fig. 1(b)]. We note that I_{LDP} may be also limited by ion acoustic turbulence (IAT) [31], which for the LDP parameters limits I_{LDP} to $\sim$100–200 kA.

The present measurements demonstrate that, in the presence of B_z, much of the current flows at large radii in a slowly imploding, low-density plasma. Here, we show that these findings can explain the unpredicted and unexplained phenomena observed in previous studies of B_z compression [7–9,11,17–19,32,33]. For example: (i) B_z

significantly slows down the plasma implosion and increases the final stagnation radius [18,19], while simulations using the NRL 1D radiation-MHD code [34] predict that the B_z counterpressure is too low to have such significant impact on the plasma dynamics. In our experiment, the implosion time for $B_{z0} = 0.4$ T is ~35% longer than for $B_{z0} = 0$, while simulations, assuming the entire current flows in the imploding plasma, predict an implosion longer by only ~2%. (ii) A very small $B_{z0} = 0.28$ T relative to the B_θ generated by the discharge current, practically eliminates the x-ray yield in the experiment on the 2.5-MA GIT-12 generator [11]. (iii) A relative very small $B_{z0} = 0.1$–0.2 T significantly stabilizes the implosion and stagnation in our experiment [18], and in the experiments on the 0.9-MA COBRA [32] and 1-MA ZEBRA facilities [33]. (iv) Unexpectedly large pitch angle of the helix-like plasma structures is observed in the magnetized liner inertial fusion experiments [17]. Assuming the observed plasma structure is generated at the outer radius of the imploding plasma and is along $\vec{B}$, a very small pitch angle is expected since $B_\theta \gg B_{z0}$. We suggest that the large pitch angle is induced by two processes: the reduced fraction of discharge current that flows in the imploding plasma, and an amplification of B_z due to an azimuthal current density (j_θ) in the LDP (that might be present outside the liner due to liner evaporation or plasma from electrodes), as explained below. We note that the possibility of current flow in peripheral plasma of the magnetized liner inertial fusion experiment has been already suggested [35], together with a mechanism, that is different from the one outlined here, to explain the large pitch angle.

The properties of the peripheral plasmas, which might have shunted current from the imploding plasma, are not known in the experiments mentioned above, nor known is the fraction of the current flow outside this plasma. The present Letter demonstrates that such Zeeman-effect measurements might be essential for revealing small fractions (~10%) of current loss to the LDP, while they cannot be inferred from the plasma implosion time (as commonly done), although such current losses can significantly affect the final stagnating plasma properties.

We suggest a possible explanation of this phenomenon. It is known [36] that plasma in constant and uniform electric ($\vec{E}$) and magnetic ($\vec{B}$) fields, which are perpendicular (i.e., $B_{z0} = 0$), reaches the drift velocity $\vec{v}_{\text{drift}} = (\vec{E} \times \vec{B})/B^2$. At this velocity, the effective electric field $\vec{E}_{\text{eff}} = \vec{E} + \vec{v} \times \vec{B}$ vanishes, and j_z is driven only by spatial gradients of the plasma parameters. For $B_{z0} = 0$, the current in the LDP due to the gradients in the plasma properties is very small and the entire current can flow in the imploding plasma. This situation changes when $B_{z0} > 0$, since at v_{drift}, $\vec{E}_{\text{eff}} \neq 0$, allowing current flow in the LDP. This can be seen from the generalized Ohm's law for constant $\vec{E} = E_z \hat{z}$, and $\vec{B} = B_\theta \hat{\theta} + B_z \hat{z}$:

$$\frac{\partial \vec{j}}{\partial t} = \frac{\nu_{\text{ei}}}{\eta}(\vec{E} + \vec{v} \times \vec{B}) - \nu_{\text{ei}}\vec{j} - \omega_{\text{ce}}\frac{\vec{j} \times \vec{B}}{|\vec{B}|}, \quad (1)$$

where $\vec{v}$ is the plasma velocity, its evolution is given by $\partial \vec{v}/\partial t = \vec{j} \times \vec{B}/\rho$ (ν_{ei} as electron-ion collision frequency, ω_{ce} as electron cyclotron frequency, and η as plasma resistivity). The pressure terms are omitted since, for the LDP conditions, $\beta \sim 10^{-2}$–10^{-1}. The steady-state solution of Eq. (1) is the force-free current configuration, $j_z = (E_z/\eta)(B_z/B)^2$, $j_\theta = (E_z/\eta)B_z B_\theta/B^2$, and $v_r = v_{\text{drift}}$, which for the LDP parameters is reached on timescales [36] of $\tau_{\text{steady}} = \nu_{\text{ei}}/(\omega_{\text{ce}}\omega_{\text{ci}}) \sim 10$–30 ns ($\omega_{\text{ci}}$ is ion cyclotron frequency) that is much shorter than the characteristic implosion time (hundreds ns). Note that j_θ in the LDP generates an additional B_z flux in the LDP and in the imploding plasma.

While the LDP plasma carries a large fraction of the current, no significant inward motion of this plasma is observed. Indeed, by estimating the v_{drift} of the LDP for $E_{z,\text{LDP}} \sim 1.5 \times 10^4$ V/m (using Spitzer resistivity and assuming uniform current distribution for $I_{z,\text{LDP}} \sim 200$ kA and $20 \leq r_{\text{LDP}} \leq 27$ mm) and $B_z \sim B_\theta \sim 1$ T, yields $v_{\text{drift}} \sim 7.5 \times 10^5$ cm/s that is small compared to the imploding plasma velocity, $v_{\text{imp}} \approx 3 \times 10^6$ cm/s. This discussion does not apply for the imploding plasma since the assumptions of constant $\vec{E}$ and $\vec{B}$ ($\tau_{\text{steady}} \sim t_{\text{implosion}} \sim 1$ μs) and the neglect of the pressure terms are not valid there.

We emphasize that the development of the force-free configuration in LDP is suggested here only as a possibility. To test this explanation requires further measurements, in particular investigation of a B_z increase due to possible j_θ in the LDP. In addition, three-dimensional modeling that involves processes beyond MHD is required to explain the observed phenomena and to test our hypothesis. Simulations of this kind have been recently published [37,38].

As said above, the significant effects of B_{z0} on the implosion dynamics are due to current loss to the LDP, and thus occur at B_{z0} values much lower than required for affecting the implosion dynamics, based on the compressed-B_z-pressure considerations. The values of B_{z0} (relative to B_θ) in the various experiments that affect significantly the implosion dynamics require further investigations; it depends on the geometry, the resistivity of the imploding plasma and the LDP, and on the LDP properties relevant to IAT or to the force-free current timescale. For example, in our experiment, it was found that ~10× reduction of the LDP density, obtained by moving the Helmholtz coils outside of the vacuum chamber, together with a few initial discharges to clean the electrodes from adsorbates, almost eliminated the current conduction through the LDP for B_{z0} up to 0.3 T, also consistent with IAT estimates. The present results demonstrate that a LDP, which may inevitably be present in high-power systems due to various processes, can affect severely the current

distribution, and possibly lead to the development of force-free configurations.

---

*Corresponding author.
Dimitry.Mikitchuk@weizmann.ac.il

[1] T. A. Mehlhorn, IEEE Trans. Plasma Sci. **42,** 1088 (2014).

[2] J. L. Giuliani and R. J. Commisso, IEEE Trans. Plasma Sci. **43,** 2385 (2015).

[3] M. R. Gomez et al., Phys. Rev. Lett. **113,** 155003 (2014).

[4] O. V. Gotchev, P. Y. Chang, J. P. Knauer, D. D. Meyerhofer, O. Polomarov, J. Frenje, C. K. Li, M. J.-E. Manuel, R. D. Petrasso, J. R. Rygg, F. H. Séguin, and R. Betti, Phys. Rev. Lett. **103,** 215004 (2009).

[5] J. O. Stenflo, Astron. Astrophys. **517,** A37 (2010).

[6] S. A. Slutz, M. C. Herrmann, R. A. Vesey, A. B. Sefkow, D. B. Sinars, D. C. Rovang, K. J. Peterson, and M. E. Cuneo, Phys. Plasmas **17,** 056303 (2010).

[7] F. S. Felber, F. J. Wessel, N. C. Wild, H. U. Rahman, A. Fisher, C. M. Fowler, M. A. Liberman, and A. L. Velikovich, J. Appl. Phys. **64,** 3831 (1988).

[8] F. S. Felber, M. M. Malley, F. J. Wessel, M. K. Matzen, M. A. Palmer, R. B. Spielman, M. A. Liberman, and A. L. Velikovich, Phys. Fluids **31,** 2053 (1988).

[9] R. K. Appartaim and A. E. Dangor, J. Appl. Phys. **84,** 4170 (1998).

[10] G. G. Zukakishvili, K. N. Mitrofanov, E. V. Grabovskii, and G. M. Oleinik, Plasma Phys. Rep. **31,** 652 (2005).

[11] A. V. Shishlov, R. B. Baksht, S. A. Chaikovsky, A. V. Fedunin, F. I. Fursov, V. A. Kokshenev, N. E. Kurmaev, A. Yu. Labetsky, V. I. Oreshkin, N. A. Ratakhin, A. G. Russkikh, and S. V. Shlykhtun, Laser Phys. **16,** 183 (2006).

[12] J. P. Knauer, O. V. Gotchev, P. Y. Chang, D. D. Meyerhofer, O. Polomarov, R. Betti, J. A. Frenje, C. K. Li, M. J.-E. Manuel, R. D. Petrasso, J. R. Rygg, and F. H. Séguin, Phys. Plasmas **17,** 056318 (2010).

[13] P. Y. Chang, G. Fiksel, M. Hohenberger, J. P. Knauer, R. Betti, F. J. Marshall, D. D. Meyerhofer, F. H. Séguin, and R. D. Petrasso, Phys. Rev. Lett. **107,** 035006 (2011).

[14] M. Hohenberger, P.-Y. Chang, G. Fiksel, J. P. Knauer, R. Betti, F. J. Marshall, D. D. Meyerhofer, F. H. Séguin, and R. D. Petrasso, Phys. Plasmas **19,** 056306 (2012).

[15] F. S. Felber, M. A. Liberman, and A. L. Velikovich, Phys. Fluids **31,** 3675 (1988).

[16] F. S. Felber, M. A. Liberman, and A. L. Velikovich, Phys. Fluids **31,** 3683 (1988).

[17] T. J. Awe et al., Phys. Rev. Lett. **111,** 235005 (2013).

[18] D. Mikitchuk, C. Stollberg, R. Doron, E. Kroupp, Y. Maron, H. R. Strauss, A. L. Velikovich, and J. L. Giuliani, Trans. Plasma Sci. **42,** 2524 (2014).

[19] A. G. Rousskikh, A. S. Zhigalin, V. I. Oreshkin, V. Frolova, A. L. Velikovich, G. Yu. Yushkov, and R. B. Baksht, Phys. Plasmas **23,** 063502 (2016).

[20] G. Davara, L. Gregorian, E. Kroupp, and Y. Maron, Phys. Plasmas **5,** 1068 (1998).

[21] R. P. Golingo, U. Shumlak, and J. Den Hartog, Rev. Sci. Instrum. **81,** 126104 (2010).

[22] G. Rosenzweig, E. Kroupp, A. Fisher, and Y. Maron, J. Instrum. **12,** P09004 (2017).

[23] V. V. Ivanov, A. A. Anderson, D. Papp, A. L. Astanovitskiy, V. Nalajala, and O. Dmitriev, Phys. Plasmas **22,** 092710 (2015).

[24] R. Doron, D. Mikitchuk, C. Stollberg, G. Rosenzweig, E. Stambulchik, E. Kroupp, Y. Maron, and D. A. Hammer, High Energy Density Phys. **10,** 56 (2014).

[25] F. C. Jahoda, F. L. Ribe, and G. A. Sawyer, Phys. Rev. **131,** 24 (1963).

[26] N. J. Peacock and B. A. Norton, Phys. Rev. A **11,** 2142 (1975).

[27] J. F. Seely, U. Feldman, N. R. Sheeley, Jr., S. Suckewer, and A. M. Title, Rev. Sci. Instrum. **56,** 855 (1985).

[28] T. Shikama and P. M. Bellan, Rev. Sci. Instrum. **84,** 023507 (2013).

[29] Y. Maron, A. Starobinets, V. I. Fisher, E. Kroupp, D. Osin, A. Fisher, C. Deeney, C. A. Coverdale, P. D. Lepell, E. P. Yu, C. Jennings, M. E. Cuneo, M. C. Herrmann, J. L. Porter, T. A. Mehlhorn, and J. P. Apruzese, Phys. Rev. Lett. **111,** 035001 (2013).

[30] See Supplemental Material at http://link.aps.org/supplemental/10.1103/PhysRevLett.122.045001 contains: 1) Azimuthal magnetic field measurements at different z-positions, 2) measurements of the low-density plasma properties, 3) measurements of the evolution of the initial axial magnetic field at different radial positions, and 4) measurements of the discharge current evolution for shots with and without axial magnetic field.

[31] D. D. Ryutov, M. S. Derzon, and M. K. Matzen, Rev. Mod. Phys. **72,** 167 (2000).

[32] N. Qi, P. de Grouchy, P. C. Schrafel, L. Atoyan, W. M. Potter, A. D. Cahill, P.-A. Gourdain, J. B. Greenly, D. A. Hammer, C. L. Hoyt, B. R. Kusse, S. A. Pikuz, and T. A. Shelkovenko, AIP Conf. Proc. **1639,** 51 (2014).

[33] F. Conti, J. Valenzuela, M. P. Ross, J. Narkis, F. Beg, H. Rahman, E. Ruskov, A. Anderson, and A. Covington, Int. Conf. Plasma Sci., 2018.

[34] J. Davis, J. L. Giuliani, Jr., and M. Mulbrandon, Phys. Plasmas **2,** 1766 (1995).

[35] D. D. Ryutov, T. J. Awe, S. B. Hansen, R. D. McBride, K. J. Peterson, D. B. Sinars, and S. A. Slutz, AIP Conf. Proc. **1639,** 63 (2014).

[36] L. Spitzer, *Physics of Fully Ionized Gases* (Courier Corporation, Mineola, New York, 2006).

[37] C. E. Seyler, M. R. Martin, and N. D. Hamlin, Phys. Plasmas **25,** 062711 (2018).

[38] A. B. Sefkow, Bull. Am. Phys. Soc. **61,** 2016.

УУБ
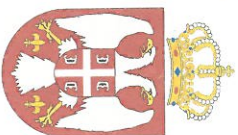
Република Србија

Универзитет у Београду
Електротехнички факултет, Београд

Диплома

Марко, Бранко, Цвејић

рођен 9. августа 1982. године у Пожаревцу, Република Србија, уписан школске
2008/2009. године, а дана 26. септембра 2014. године завршио је докторске академске
студије, трећег степена, на студијском програму Електротехника и рачунарство,
обима 180 (сто осамдесет) бодова ЕСПБ са просечном оценом 10,00 (десет и 0/100).

Наслов докторске дисертације је: „Просторна и временски
разложена спектроскопска ласерски индуковане
плазме на чврстој мети у ваздуху на атмосферском притиску".

На основу тога издаје му се ова диплома о стеченом научном називу

доктор наука - електротехника и рачунарство

Број: 3776500
У Београду, 21. маја 2015. године

Декан
Проф. др Бранко Ковачевић

Ректор
Проф. др Владимир Бумбаширевић

Република Србија
МИНИСТАРСТВО ПРОСВЕТЕ,
НАУКЕ И ТЕХНОЛОШКОГ РАЗВОЈА
Комисија за стицање научних звања

Број:660-01-00042/609
25.03.2015. године
Б е о г р а д

На основу члана 22. става 2. члана 70. став 5. Закона о научноистраживачкој делатности ("Службени гласник Републике Србије", број 110/05 и 50/06 – исправка и 18/10), члана 2. става 1. и 2. тачке 1 – 4.(прилози) и члана 38. Правилника о поступку и начину вредновања и квантитативном исказивању научноистраживачких резултата истраживача ("Службени гласник Републике Србије", број 38/08) и захтева који је поднео

Институт за физику у Београду

Комисија за стицање научних звања на седници одржаној 25.03.2015. године, донела је

ОДЛУКУ
О СТИЦАЊУ НАУЧНОГ ЗВАЊА

Др Марко Цвејић

стиче научно звање
Научни сарадник

у области природно-математичких наука - физика

О Б Р А З Л О Ж Е Њ Е

Институт за физику у Београду

утврдио је предлог број 1648/1 од 09.12.2014. године на седници научног већа Института и поднео захтев Комисији за стицање научних звања број 1700/1 од 18.12.2014. године за доношење одлуке о испуњености услова за стицање научног звања *Научни сарадник*.

Комисија за стицање научних звања је по претходно прибављеном позитивном мишљењу Матичног научног одбора за физику на седници одржаној 25.03.2015. године разматрала захтев и утврдила да именовани испуњава услове из члана 70. став 5. Закона о научноистраживачкој делатности ("Службени гласник Републике Србије", број 110/05 и 50/06 – исправка и 18/10), члана 2. става 1. и 2. тачке 1 – 4.(прилози) и члана 38. Правилника о поступку и начину вредновања и квантитативном исказивању научноистраживачких резултата истраживача ("Службени гласник Републике Србије", број 38/08) за стицање научног звања *Научни сарадник,* па је одлучила као у изреци ове одлуке.

Доношењем ове одлуке именовани стиче сва права која му на основу ње по закону припадају.

Одлуку доставити подносиоцу захтева, именованом и архиви Министарства просвете, науке и технолошког развоја у Београду.

ПРЕДСЕДНИК КОМИСИЈЕ   **ДРЖАВНИ СЕКРЕТАР**
Др Станислава Стошић-Грујичић,   Др Александар Белић
научни саветник